

Development and demonstration of a Lagrangian dispersion modeling system for real-time prediction of smoke haze pollution from biomass burning in Southeast Asia

Article

Published Version

Hertwig, D. ORCID: <https://orcid.org/0000-0002-2483-2675>, Burgin, L., Gan, C., Hort, M., Jones, A., Shaw, F., Witham, C. and Zhang, K. (2015) Development and demonstration of a Lagrangian dispersion modeling system for real-time prediction of smoke haze pollution from biomass burning in Southeast Asia. *Journal of Geophysical Research: Atmospheres*, 120 (24). pp. 12605-12630. ISSN 2169-8996 doi: <https://doi.org/10.1002/2015JD023422> Available at <https://centaur.reading.ac.uk/76901/>

It is advisable to refer to the publisher's version if you intend to cite from the work. See [Guidance on citing](#).

To link to this article DOI: <http://dx.doi.org/10.1002/2015JD023422>

Publisher: American Geophysical Union

including copyright law. Copyright and IPR is retained by the creators or other copyright holders. Terms and conditions for use of this material are defined in the [End User Agreement](#).

www.reading.ac.uk/centaur

CentAUR

Central Archive at the University of Reading

Reading's research outputs online

RESEARCH ARTICLE

10.1002/2015JD023422

Key Points:

- Lagrangian modeling of smoke haze dispersion with wildfire emission inventories
- Established confidence in use of modeling system as quantitative forecast tool
- Detailed representation of peat and cloud cover correction improves accuracy

Supporting Information:

- Figure S1

Correspondence to:

L. Burgin,
laura.burgin@metoffice.gov.uk

Citation:

Hertwig, D., L. Burgin, C. Gan, M. Hort, A. Jones, F. Shaw, C. Witham, and K. Zhang (2015), Development and demonstration of a Lagrangian dispersion modeling system for real-time prediction of smoke haze pollution from biomass burning in Southeast Asia, *J. Geophys. Res. Atmos.*, 120, 12,605–12,630, doi:10.1002/2015JD023422.

Received 9 APR 2015

Accepted 24 NOV 2015

Accepted article online 28 NOV 2015

Published online 22 DEC 2015

©2015. The American Geophysical Union and Crown copyright. This article is published with the permission of the Controller of HMSO and the Queen's Printer for Scotland.

Development and demonstration of a Lagrangian dispersion modeling system for real-time prediction of smoke haze pollution from biomass burning in Southeast Asia

Denise Hertwig¹, Laura Burgin¹, Christopher Gan², Matthew Hort¹, Andrew Jones¹, Felicia Shaw², Claire Witham¹, and Kathy Zhang²

¹Met Office, Exeter, UK, ²Meteorological Service Singapore, Singapore

Abstract Transboundary smoke haze caused by biomass burning frequently causes extreme air pollution episodes in maritime and continental Southeast Asia. With millions of people being affected by this type of pollution every year, the task to introduce smoke haze related air quality forecasts is urgent. We investigate three severe haze episodes: June 2013 in Maritime SE Asia, induced by fires in central Sumatra, and March/April 2013 and 2014 on mainland SE Asia. Based on comparisons with surface measurements of PM₁₀ we demonstrate that the combination of the Lagrangian dispersion model NAME with emissions derived from satellite-based active-fire detection provides reliable forecasts for the region. Contrasting two fire emission inventories shows that using algorithms to account for fire pixel obscuration by cloud or haze better captures the temporal variations and observed persistence of local pollution levels. Including up-to-date representations of fuel types in the area and using better conversion and emission factors is found to more accurately represent local concentration magnitudes, particularly for peat fires. With both emission inventories the overall spatial and temporal evolution of the haze events is captured qualitatively, with some error attributed to the resolution of the meteorological data driving the dispersion process. In order to arrive at a quantitative agreement with local PM₁₀ levels, the simulation results need to be scaled. Considering the requirements of operational forecasts, we introduce a real-time bias correction technique to the modeling system to address systematic and random modeling errors, which successfully improves the results in terms of reduced normalized mean biases and fractional gross errors.

1. Introduction

Smoke haze resulting from hundreds of simultaneously emitting wildfires regularly deteriorates air quality in Southeast Asia and can result in particularly hazardous conditions in densely populated urban areas. The large-scale burning of biomass (e.g., forests, crop residue, or peat) is mostly of anthropogenic origin. Resulting emissions of particulate aerosols and greenhouse gases, including carbon dioxide and methane, into the atmosphere are of great environmental and political concern regarding the short- and long-term consequences for human health [e.g., Emmanuel, 2000; Kunii et al., 2002; Frankenberger et al., 2005; Marlier et al., 2013], the stability of local ecosystems [e.g., Nichol, 1997; Balasubramanian et al., 1999; Taylor, 2010], and global climate change [e.g., Goldammer, 1997; Heil and Goldammer, 2001; Page et al., 2002; van der Werf et al., 2004].

Though now illegal, deforestation and land clearing through fires are commonly seen in the region. Local fires often escalate into uncontrollable large-scale environmental catastrophes that also affect air quality in neighboring countries through long-range transport of pollutants [e.g., Taylor, 2010; Jones, 2006]. This is usually referred to as transboundary smoke haze. Since 2002, member states of the Association of Southeast Asian Nations have been promoting a zero-burning policy as part of the "Agreement on Transboundary Haze Pollution," with Indonesia being the last member country to ratify the agreement in September 2014 (haze.asean.org) [Jones, 2006]. The periodic reoccurrence of smoke haze problems in Southeast Asia, however, shows that enforcing these regulations has not yet cascaded down to all entities. This is a particular problem in Indonesia, where fires, especially in Sumatra and Kalimantan, Borneo, are continuing to escalate almost on a yearly basis and prevention and mitigation efforts so far have had limited effect [Jones, 2006; Lohman et al., 2007; Hansen et al., 2013; Reid et al., 2012, 2013; Kim et al., 2015]. Based on a comprehensive publication survey, Streets et al. [2003] estimate that approximately 330 Tg of biomass

are burnt in Southeast Asia in an average year, with forest fires playing a dominant role. However, such quantitative estimates are associated with large degrees of uncertainty [e.g., *Hyer et al.*, 2013; *Reid et al.*, 2013].

Air-pollution problems related to fires are also encountered in continental Southeast Asia. Every year during the dry season from October to April highland forests and croplands in North Thailand, Myanmar, Laos, Vietnam, and Cambodia suffer from burning on large scales, resulting in prolonged spells of poor air quality, particularly in the premonsoon months of March and April [e.g., *Stott*, 1986; *Hoare*, 2004; *Sirimongkonlertkul and Phonekeo*, 2012; *Gautam et al.*, 2013]. Transboundary smoke haze from these fires can also affect faraway areas in Southern China, the South China Sea, and the Taiwan Strait [*Huang et al.*, 2013].

The potential of local fires to develop beyond control into disastrous burns with haze affecting regions over large distances is strongly intertwined with the complex meteorology of the tropics. Both the Indian and the Australian monsoons induce seasonal shifts in wind regimes and strong variations in precipitation intensities throughout Southeast Asia (see detailed discussions by *Lau and Yang* [1997], *Chang et al.* [2005], and *Xian et al.* [2013]). Precipitation patterns in continental Southeast Asia are governed by the Indian monsoon, inducing a wet season from May to September (details of the climatology are discussed by *Zhang et al.* [2002]). However, in maritime Southeast Asia, often referred to as the Maritime Continent [*Ramage*, 1968], monsoon phases are more closely related to the Australian monsoon, with a wet season during boreal winter and a dry season during boreal summer [*Chang et al.*, 2005]. This annual cycle, however, is subject to strong local variations due to the complex distribution of land, sea, and terrain.

Giglio et al. [2006] have identified typical fire patterns in maritime Southeast Asia, with the peak activity starting in Sumatra and continuously shifting eastward during the dry season from July to October. *Xian et al.* [2013] showed that from June to September smoke aerosols emitted in central and southern Sumatra and southern and western Borneo are typically transported north-eastward with the cross-equatorial flow. Fire activity typically ceases with the onset of the winter monsoon and associated high rainfall rates in October/November.

In their multiyear analysis of fire hot spots in the Maritime Continent, *Reid et al.* [2012] presented a comprehensive overview of the influence of multiscale meteorological phenomena on the bulk seasonal and short-term fire activity in the Maritime Continent. Wildfire intensities can, for example, be significantly amplified by the El Niño–Southern Oscillation (ENSO) [see also *Heil and Goldammer*, 2001; *van der Werf et al.*, 2004; *Fuller and Murphy*, 2006] and/or the Indian Ocean Dipole (IOD) [e.g., *Field et al.*, 2009], leading to strong emission anomalies. Unprecedented levels of smoke haze originating from Sumatra and Kalimantan occurred during the strong 1997 to 1998 El Niño-induced drought period [e.g., *Heil and Goldammer*, 2001; *Koe et al.*, 2001; *Kunii et al.*, 2002]. *Page et al.* [2002] estimated that during this prolonged burning episode the equivalent of 13 to 40% of the mean annual global carbon emissions from fossil fuels were emitted from the Indonesian archipelago.

High hot spot counts continue to be encountered every year in Sumatra and Kalimantan (see recent studies by *Yulianti et al.* [2013], *Atwood et al.* [2013], and *Reddington et al.* [2014]). Peat fires in eastern central and southeastern Sumatra, primarily lit for converting land to palm oil plantations, are particularly detrimental for air quality in major cities in the Maritime Continent [*Kim et al.*, 2015]. *Reid et al.* [2012] have shown that wildfires in central Sumatra are more independent of the ENSO phase: Smoke haze pollution from this region can occur throughout the year as a result of land-clearing activities and crop residue burning during any period of prolonged dry weather conditions.

As an example, in June 2013 Singapore and its surrounding regions were blanketed by thick smoke haze that was transported across the Strait of Malacca by anomalous, strong westerly winds that were enhanced by the presence of a tropical cyclone in the South China Sea (Figure 1). The severe pollution episode was caused by agricultural fires in the eastern part of central Sumatra (mainly Riau Province). These fires were lit following a dry spell during non-El Niño and IOD-neutral conditions just before the onset of the usual haze season [*Kopplitz et al.*, 2014]. Within the short period between the 11 and 30 June 2013, the air quality monitoring network in Singapore recorded the worst wildfire-induced air quality degradation in its history, with pollution levels exceeding the records of the 1997/1998 haze. The 24 h Pollutant Standards Index (PSI) issued by Singapore's National Environment Agency, an index calculated from a range of pollutants including particulate matter (<http://www.nea.gov.sg/anti-pollution-radiation-protection/air-pollution-control/psi>), indicated “unhealthy” to “very unhealthy” air quality conditions between 17 and 23 June with a record high of 246 being reached on 22 June [*National Environment Agency*, 2013].

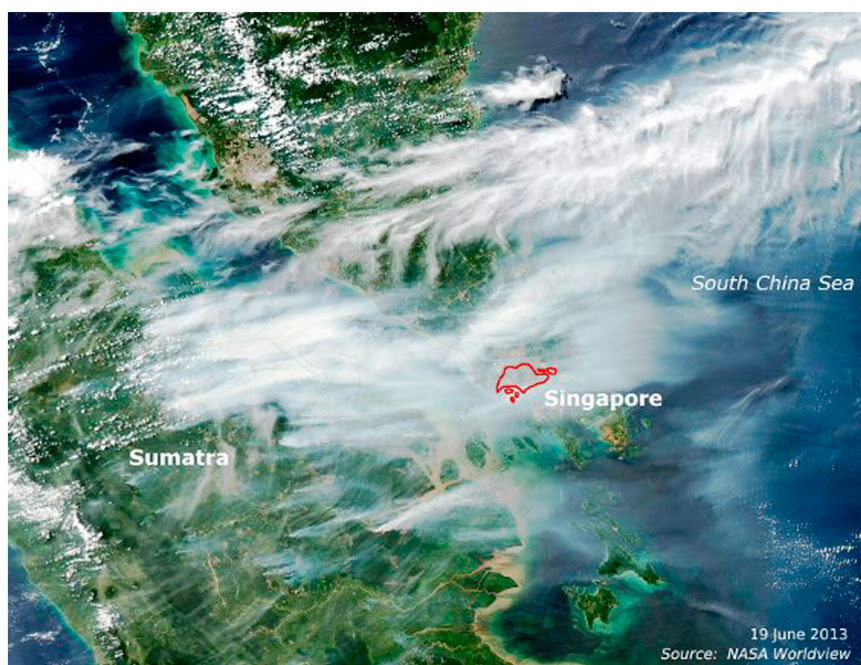


Figure 1. Transboundary smoke haze plumes originating from central Sumatran wildfires on 19 June 2013, shortly before record pollution conditions were reached in Singapore (source: NASA Worldview).

Gaveau *et al.* [2014] report that in the two months prior to the outbreak of the fires, deficits in the monthly rainfall rates were registered in central Sumatra in an otherwise wetter than usual year. Their investigations showed that June 2013 saw the largest monthly release of Fire Radiative Power (FRP) ever detected by the Moderate Resolution Imaging Spectroradiometer (MODIS) on board NASA's polar-orbiting Terra and Aqua satellites. The bulk of FRP was found to have been generated on land that had already been deforested in recent years. 84% of the estimated 163,336 ha of burnt landscape was drained peatland.

Tropical peat soil is a major reserve of organic carbon [Page *et al.*, 2002]. Its burning typically results in persistent smouldering fires that can lead to higher emission levels of greenhouse gases and, through incomplete combustion, of particulate matter compared to vegetation fires [e.g., Christian *et al.*, 2003; Heil *et al.*, 2007; van der Werf *et al.*, 2010]. In recent years, the most fire-prone areas in the Maritime Continent were observed to be located in peat areas along the eastern coast of Sumatra and southern Kalimantan [Yulianti and Hayasaka, 2013; Yulianti *et al.*, 2013]. These areas have also been subject to rapid deforestation, conversion to plantations, and degradation into secondary vegetation [Miettinen *et al.*, 2011].

1.1. Scope of This Study

Reacting to the June 2013 event, the Met Office of the United Kingdom and the Hazard Risk and Impact Assessment Unit of the Meteorological Service Singapore (MSS) have explored how to adequately simulate haze pollution dispersion in this region, with the particular aim of setting up a reliable routine quantitative haze forecast system for Singapore. At the core of the modeling system lies the Met Office's Lagrangian particle dispersion model NAME (Numerical Atmospheric-dispersion Modelling Environment), which is driven with off-line Numerical Weather Prediction (NWP) data and high-resolution, satellite-based emission products from active-fire detection that are currently available in near real time for the region of interest.

The aim of the study is to establish confidence in the NAME haze-dispersion simulations using these quantitative wildfire emission estimates. For this purpose, near-surface predictions from the modeling system are evaluated against ground-based observations of PM_{10} that were available for recent smoke haze episodes in the region. While the primary focus is on the severe haze event affecting Singapore in June 2013, we also run the forecast demonstration system for two smoke haze episodes in North Thailand occurring in March/April 2013 and 2014. Analyzing events in both maritime and continental Southeast Asia offers a better appreciation of deficiencies of individual components of the modeling system, as meteorological, orographic, and biomass-burning features (e.g., in terms of typical fuel types) differ vastly between these regions. The results

of this study are interpreted with regard to further optimizations of model components that are expected to increase the skill of local and regional smoke haze predictions.

Finally, we explore real-time bias correction strategies for implementation within an operational smoke haze dispersion forecast product for Singapore. The bias correction method used here is a pragmatic approach designed to optimize predictions of localized near-surface concentrations based on available real-time observations.

2. Models and Data

2.1. Satellite-Based Emission Inventories

In many parts of the world where surface observations are limited, such as the Maritime Continent, satellites provide the most comprehensive way to measure fire activity and resulting emissions. In recent years, fire hot spot detections, burnt-area estimates, and FRP measurements have been commonly used as the basis to estimate the quantity of burnt biomass. The linear relationship between time-integrated FRP and biomass combustion rate was demonstrated by *Wooster et al.* [2005]. From there, empirically derived emission factors can be applied to calculate emission rates for various smoke constituents. *Ichoku and Kaufman* [2005] and *Ichoku and Ellison* [2014] have also examined the direct relationship between FRP and emissions of smoke aerosols. Some widely used emission inventories are the Global Fire Emissions Database (GFED) [*van der Werf et al.*, 2010], Fire INventory of NCAR (FINN) [*Wiedinmyer et al.*, 2011], Quick Fire Emission Dataset (QFED) [*Darmenov and da Silva*, 2013], and the Global Fire Assimilation System (GFAS) [*Kaiser et al.*, 2012]. GFED relies on estimates of burnt area whereas the other systems convert active-fire measurements into emissions. As *Hyer et al.* [2013] state, active-fire detection products are the best data available for automated systems such as the one we aim to develop here. The burnt-area approach is not suitable as it does not supply data in near real time.

These emission inventories all rely on data from the polar-orbiting MODIS sensors on board Aqua and Terra [*Giglio et al.*, 2003]. MODIS data are generally available from four daily overpasses for each location on Earth, with active-fire products available at a uniform resolution of 1 km. However, MODIS pixels vary across the width of each scan from a minimum of roughly 1 km² at nadir to more than 9 km² at the scan edge, leading to a factor of 10 decrease in detection efficiency between the center and edges of the MODIS scan [*Hyer et al.*, 2013]. For our study area, other significant challenges exist in satellite detection and monitoring of fires when using polar-orbiting derived data due to the proximity to the equator. Orbital gaps at swath edges near the equator often decrease the number of available MODIS overpasses, thereby reducing the temporal availability of fire data. Furthermore, fire activity in peat areas shows a peak during the late afternoon period, but this important part of the fire diurnal cycle lacks coverage from fire-detecting polar-orbiting satellites in the Maritime Continent [*Hyer et al.*, 2013]. Low thermal signatures from smouldering peat fires burning beneath the surface also tend to be harder to detect than surface vegetation fires [*Reid et al.*, 2013], while being highly significant in terms of emissions. Finally, the highly fragmented landscape of our study area can lead to additional uncertainties in emissions calculated through the FRP method, as small errors made in locating hot spots can easily lead to the wrong land cover classification being used.

Data sets based on geostationary satellite observations are also available, providing high temporal coverage and enabling the full diurnal cycle of burning to be captured, but with reduced spatial resolution. For example, data produced by the Wildfire Automated Biomass Burning Algorithm (WF_ABBA) from the geostationary MTSAT satellite has a resolution of approximately 4 km at nadir and up to 8 km at limb viewing [*Reid et al.*, 2009]. *Hyer et al.* [2013] compared WF_ABBA data to MODIS active-fire data for the Maritime Continent. They found broad-scale similarities in spatial and temporal patterns between the data sets when aggregating data to relatively coarse resolutions of 5° in space and 16 days in time. However, correlations were low for higher resolutions that would be required for air quality forecasting. This was thought to be due to the reduced detection efficiency of the low-resolution WF_ABBA product and related errors in fire detection in heterogeneous land cover.

Hyer et al. [2013] conclude that a combination of polar-orbiting and geostationary detections of active fire are needed to create a truly quantitative estimate of biomass burning emissions in Southeast Asia. This challenge has not yet been undertaken in an automated way, but an analyst-based system is being trialed and used by NOAA for a North American forecast domain [*Rolph et al.*, 2009].

A major issue with emissions derived from both polar and geostationary satellite-based hot spot detections occurs from obscuration of fires by clouds and haze. This issue is particularly significant in our study area where abundant cloud cover, including ubiquitous high cirrus cloud, frequently obscures fires from satellite sensors (as shown by the MISR Level 3 cloud fractions presented for 2001–2010 in Reid *et al.* [2013]). Further obscuration can also be expected by thick smoke plumes during severe fire episodes. Emission inventories attempt to address this issue in different ways. GFAS corrects for partial cloud cover during a single day by assuming a uniform distribution of fires in each grid cell. A persistence algorithm is used to fill observation gaps from day to day. However, this assumption may lead to an overestimation when precipitation beneath the clouds diminishes fire activity. QFED makes use of the cloud correction method developed by GFAS but contains a complex assimilation method for completely obscured pixels [Darmenov and da Silva, 2013]. Products based on burnt-area or geostationary satellite data have the opportunity for multiple scans of the same area, reducing the likelihood of cloud contamination.

For the development of an operational smoke haze dispersion forecast system for Singapore, two biomass burning emission inventories have been used. Due to our requirement to have a near real time system that can be operated with limited computing resources and analysts, active-fire products from MODIS have been used as the basis for two tested emissions databases. (1) The GFAS v1.2 data set, which is produced operationally and available in near real time, and (2) the “MSS data set,” which is generated by incorporating updated conversion and emission factors, which will be used in the next version of GFAS [Kaiser *et al.*, 2014], and is based on higher-resolution land cover and peat maps for Southeast Asia. Given the severity of peat fire emissions and the rapid land conversion rates in Sumatra and Borneo, the accuracy of land cover and peatland maps used in the emission data sets are of great importance for the estimation of smoke emissions.

2.1.1. GFAS v1.2

GFAS v1.2 provides daily gridded global emission estimates from biomass burning at 0.1° resolution. FRP values are assimilated, and biomass burning emission estimates are produced for eight land cover classes. Corrections are applied for observation gaps and partial cloud cover through a Kalman filter and fire persistence model, and spurious observations from volcanoes, gas flares, and industrial activity are masked out [Kaiser *et al.*, 2012]. The combustion rate is subsequently calculated based on land cover-specific conversion factors that are linked to GFED v3.1 [Heil *et al.*, 2010]. Emission rates of 40 smoke constituents, including total particulate matter (TPM), are then calculated by linearly scaling the dry matter combustion rate with emission factors documented by Andreae and Merlet [2001].

As emissions for PM₁₀ are not available in GFAS v1.2, we use TPM as an approximation for PM₁₀ in our modeling since the majority of particulate emissions from biomass burning have been found to be in the accumulation mode, with only a very small fraction larger than PM₁₀ [Reid *et al.*, 2005]. Injection heights for each source are determined from a plume-rise model [Freitas *et al.*, 2007].

The 0.5° resolution land cover map used in GFAS v1.2 is derived from the dominant fire-type map in GFED v3.1 [Kaiser *et al.*, 2012]. Six of the overall eight land cover classes used in GFAS v1.2 can be found in our study area and are indicated in Figure 2. Areas with organic soil are differentiated for savannah, agriculture, and extratropical forest. Due to the dominance of peat, it is treated as an individual land cover type and surface vegetation characteristics are unaccounted for.

In this study, we defined two source domains, one focusing on the Maritime Continent and the other in mainland Southeast Asia. Both domains are indicated in Figures 2 and 3 and described in more detail in section 3.1. An overview of the GFAS v1.2 land cover classification, the area, and percentage of the total land area covered by each land cover class for the Maritime Continent and mainland Southeast Asia domains are presented in Table 1. For both domains, the dominant land cover type is tropical forest, covering 70.6% and 69% of the respective total land area. The representation of peat areas in GFAS v1.2 is based on the 0.5° peat map used in GFED v3.1 [van der Werf *et al.*, 2010]. This map only includes peat areas in Sumatra and Kalimantan. Other peat areas in Southeast Asia have been omitted. Compared with peat inventories by Wetlands International (WI) [Wahyunto and Subagio, 2003] and the Harmonised World Soil Database [Nachtergaele *et al.*, 2012], peat areas in GFAS v1.2 are much smaller in central Sumatra (Riau Province) and much larger in the provinces of South Sumatra and Lampung (see Figure 2). Thus, peat fire emissions in GFAS v1.2 are expected to be underestimated in Riau and conversely overestimated in South Sumatra and Lampung. In Kalimantan, however, there is relatively good agreement in the spatial pattern of peatland among the peat inventories.

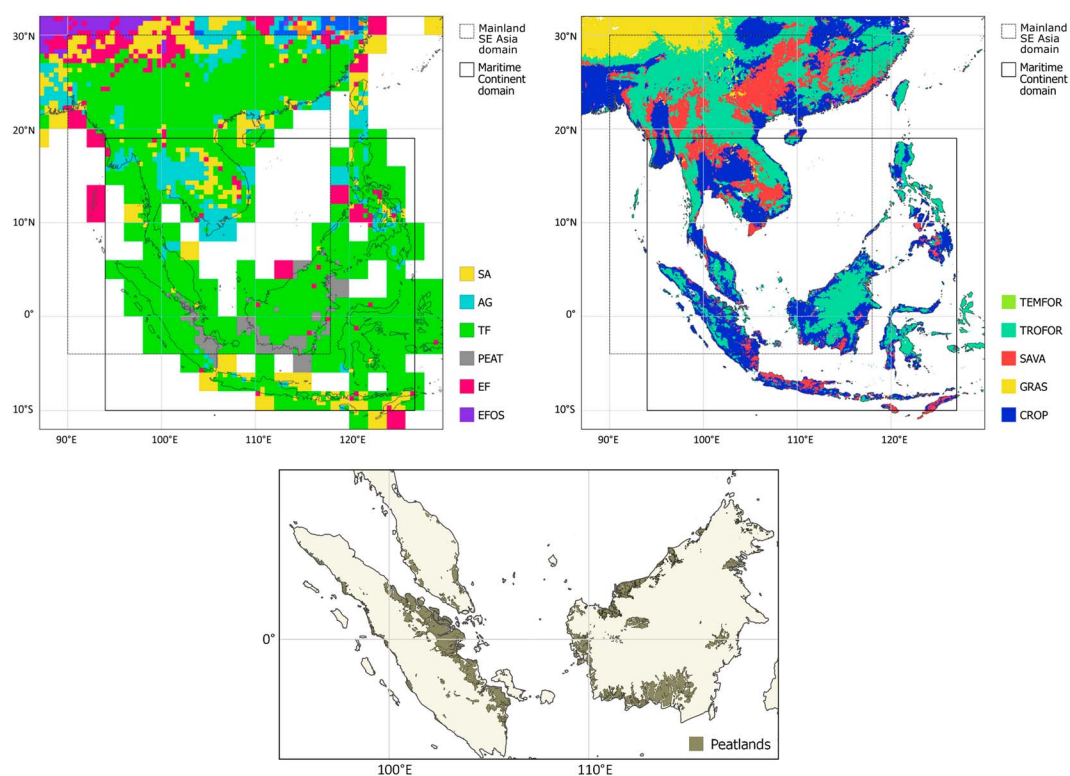


Figure 2. Land cover class maps used for (top left) GFAS v1.2 and (top right) MSS biomass-burning emission estimates. Land-type acronyms are described in Table 1. (bottom) Peatland map used in the MSS data set for areas in Sumatra, Kalimantan, Malaysia, Sabah, and Sarawak.

2.1.2. MSS Data Set

For a more detailed representation of peat in the MSS data set, we make use of the WI peatland atlases for Sumatra and Kalimantan [Wahyunto and Subagjo, 2003, 2004]. Peatland areas for Peninsular Malaysia, Sabah, and Sarawak were derived from maps available in the European Digital Archive of Soil Maps [Selvaradjou et al., 2005] and are the same as described in Miettinen et al. [2012].

Significant agricultural and plantation areas in Peninsular Malaysia, Sumatra, Borneo, and Java are notably absent in the GFAS v1.2 land cover map and are primarily represented as tropical forest (Figure 2). To improve the land cover representation for the MSS data set, we use the 250 m resolution 2010 land cover map developed by the Centre for Remote Imaging, Sensing, and Processing (CRISP) at the National University of Singapore [Miettinen et al., 2012], covering latitudes between 10°S and 10°N. We use the individual MODIS 1 km resolution active fire detection products, MOD14 and MYD14 [Giglio et al., 2003, 2006], and the CRISP map was correspondingly remapped to 1 km resolution using a nearest neighbor approach.

Land cover classifications used in the MSS data set as well as respective fractions of total land area in the Maritime Continent and mainland Southeast Asia domains are shown in Table 1. The CRISP land cover classes were translated based on the description that most closely corresponds to one of the fire-type classes presented in Kaiser et al. [2014]. Forest and mangrove areas are translated into the “tropical forest” fire type, areas comprising plantations and agriculture into “cropland,” and open areas into “savannah.” For areas north of 10°N, the 0.05° MODIS land cover type product MCD12C1 v5.1 with University of Maryland (UMD) classification is used, and the default translation scheme is applied as outlined in Kaiser et al. [2014]. In the Maritime Continent, the land cover type with the largest area is cropland, covering 46.6% of the total area, while for the mainland Southeast Asia domain it is tropical forest (42.9%). Major urban areas demarcated in the CRISP and MCD12C1 maps are used to mask spurious FRP observations from industrial installations. Known locations of volcanoes are used to filter out volcanic hot spots.

Table 1. Description of Land Cover Classification Used in GFASv1.2 and the MSS Data Set, Including the Area and Percentage of Total Land Area Covered by Each Class in the Maritime Continent and Mainland Southeast Asia Domains^a

| Land Cover Classification | | Maritime Continent Domain | | Mainland Southeast Asia Domain | |
|-------------------------------------|---|----------------------------------|------|----------------------------------|------|
| Abbreviation | Description | ×10 ⁶ km ² | % | ×10 ⁶ km ² | % |
| <i>GFAS v1.2 Emission Inventory</i> | | | | | |
| SA | savannah | 0.25 | 7.7 | 0.55 | 9.5 |
| AG | agriculture | 0.44 | 13.4 | 0.66 | 11.4 |
| TF | tropical forest | 2.30 | 70.6 | 3.98 | 69.0 |
| PEAT | peat | 0.21 | 6.5 | 0.20 | 3.4 |
| EF | extratropical forest | 0.06 | 1.9 | 0.36 | 6.2 |
| EFOS | extratropical forest with organic soil | 0.00 | 0.0 | 0.02 | 0.4 |
| <i>MSS Emission Inventory</i> | | | | | |
| TEMFOR | temperate forest | 0.0 | 0.0 | 0.01 | 0.2 |
| TROFOR ^b | tropical forest | 1.18 | 36.4 | 2.47 | 42.9 |
| SAVA ^c | savannah | 0.51 | 15.6 | 1.21 | 21.0 |
| GRAS | grassland | 0.02 | 0.6 | 0.29 | 5.0 |
| CROP ^d | cropland | 1.51 | 46.6 | 1.74 | 30.3 |

^aIn the MSS data set the detailed CRISP land cover types were translated into more general fire types described in Kaiser *et al.* [2014].

^bIncluding mangrove, peat swamp forest, lowland forest, lower/upper montane forest.

^cIncluding lowland/montane open.

^dIncluding plantation/regrowth, lowland/montane mosaic, and large-scale palm plantation.

On top of the fire-type classes, conversion factors differentiated for peat and nonpeat areas are used to obtain combustion rates [Kaiser *et al.*, 2014], accounting for vegetation characteristics of peat areas. Emission rates for PM₁₀ are then calculated for each source using emission factors for TPM based on Akagi *et al.* [2011].

Instead of using a plume-rise model as in GFAS v1.2, a fixed injection height of 800 m was chosen based on the findings of Tosca *et al.* [2011] and Wang *et al.* [2013]. Furthermore, no correction or fire persistence algorithms for observation gaps and obstruction of fire pixels due to cloud or haze were applied during the construction of the MSS emissions inventory.

2.2. Dispersion Modeling

Wildfire emissions have been widely included in global climate and atmospheric chemistry models, and strong effort has been put into parameterizing and integrating the disparate processes involved in biomass burning and transport [e.g., Byun and Schere, 2006; Strand *et al.*, 2012; Xian *et al.*, 2013; Kim *et al.*, 2015].

In recent years, a number of NWP centers have moved toward the development and integration of aerosol modeling in their operational systems. Operational or semioperational aerosol forecasts are now available from several state-of-the-art aerosol prediction systems including the U.S. Navy Aerosol Analysis and Prediction System model (NAAPS) [Zhang *et al.*, 2008; Xian *et al.*, 2009], the European Centre for Medium-Range Weather Forecasts (ECMWF) Monitoring Atmospheric Composition and Climate model (MACC) [Morcrette *et al.*, 2009; Benedetti *et al.*, 2009], the Japan Meteorological Agency (JMA) Model of Aerosol Species in the Global Atmosphere (MASINGAR) [Tanaka *et al.*, 2003], and the NASA Global Modelling and Assimilation Office (GMAO) Goddard Earth Observing System Version 5 (GEOS-5) [Rienecker *et al.*, 2008]. All of these models include some form of satellite data assimilation, but not surface observations of particulate matter. Furthermore, a global multimodel aerosol forecasting ensemble has been developed under the International Cooperative for Aerosol Prediction (ICAP), which incorporates the aforementioned models as members [Sessions *et al.*, 2015]. Predictions of AOT at Singapore were shown to be underestimated by the models when comparing with the Singapore AERONET site [Sessions *et al.*, 2015].

A variety of bottom-up and top-down approaches to deriving emissions are employed in these global operational systems. One common aspect among these different emission inventories is that they draw from MODIS

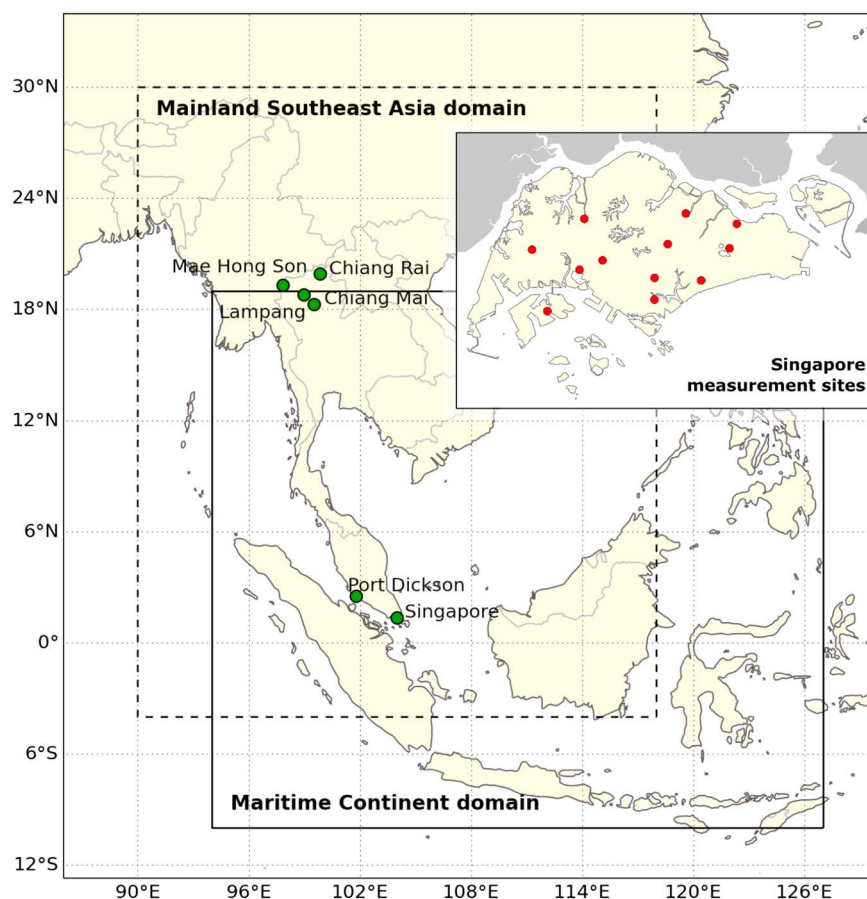


Figure 3. Locations of ground-based PM_{10} measurement sites analyzed in this study. Concentrations are reported as 24-hour averaged values at all locations except for Singapore. Here hourly-averaged concentrations are available at 12 urban sites (detailed map). The extents of the sources domains defined for the case studies are also indicated.

fire detections, though the Fire Locating and Modelling of Burning Emissions dataset (FLAMBE) [Reid *et al.*, 2009] used in the NAAPS model also assimilates data from geostationary satellites.

As peat fires are a key source of smoke haze in Southeast Asia, the specific treatment of their emissions is an important consideration. Many of the worst smoke haze events in Southeast Asia have been associated with burning in peatland areas [Reid *et al.*, 2013]. While GFAS differentiates between fires in peat and nonpeat areas, other global emission inventories (e.g., FLAMBE and QFED) do not explicitly account for peat fires. While the drawbacks of using a satellite-based FRP approach are well documented [Reid *et al.*, 2013; Kaiser *et al.*, 2012], the explicit inclusion of peat fire emissions is a critical factor in our selection of the GFAS data set in this study, given the nature of smoke haze sources in the region.

The current suite of available operational aerosol forecast systems comprise Eulerian (NAAPS and GEOS-5) and semi-Lagrangian (MACC and MASINGAR) models. In such models, complex calculations performed to work out species concentrations at each time step and at all locations are computationally expensive. Consequently, this can limit the spatial and temporal resolution of these models. For example, NAAPS has a resolution of $1^\circ \times 1^\circ$ with 27 vertical levels and produces 6-hourly forecasts, MASINGAR runs at $1.125^\circ \times 1.125^\circ$ with 30 vertical levels, and GEOS-5 at $0.25^\circ \times 0.3125^\circ$ with 70 levels [Sessions *et al.*, 2015].

For our study into the feasibility of an operational smoke haze dispersion forecast for Singapore, the need for timely information about biomass-burning emissions from a large number of wildfire sources in the region currently precludes the use of a complex atmospheric chemistry model. Instead, a Lagrangian atmospheric dispersion model with its chemistry scheme switched off has been selected. The system presented is the first operational, Lagrangian-based system in Southeast Asia. The model can meet the requirements to produce high temporal and spatial forecasts of PM_{10} at ground level where health impacts are experienced and

can be verified and bias corrected against ground-based measurement stations. Such outputs are not readily available from the current global operational systems nor do they make use of surface observations in their assimilation schemes. Additionally, the Lagrangian framework allows smoke plumes to be better resolved near to source areas.

Lagrangian dispersion models are designed to predict the atmospheric transport and deposition of airborne gaseous and particulate substances, covering spatial scales from a few hundred meters to across the globe [e.g., *Lin et al.*, 2013]. Turbulent transport of pollutants in the atmosphere is modeled using a stochastic framework. Emissions from a pollutant source are simulated by creating a large number of model particles, of which each represents a certain proportion of the mass of pollutants released. These particles are advected by an ambient three-dimensional wind field with turbulent dispersion being simulated using random-walk methods. The particles can also evolve with time to account for various atmospheric processes that might transform or remove pollutants, such as radioactive decay of radionuclide species, chemical transformations, gravitational settling, or dry and wet deposition.

In this study we use the Met Office's Lagrangian atmospheric dispersion model NAME [*Jones et al.*, 2007]. This model is used in a diverse range of applications which include emergency-response modeling, routine forecasting, scientific research, and policy support work [e.g., *Webster et al.*, 2012; *Draxler et al.*, 2015]. NAME has previously been used to identify contributions to global greenhouse gases from large-scale biomass burning [*Simmonds et al.*, 2005] and for individual studies of biomass-burning transport [*Witham and Manning*, 2007; *Johnson et al.*, 2008].

2.3. Air Quality Observations

We analyze hourly-averaged PM₁₀ concentrations from 12 sites in Singapore that were acquired by Singapore's National Environment Agency through the Telemetric Air Quality Monitoring and Management System. Equipment installed at the air quality monitoring sites measures concentrations of major criteria pollutants including sulphur dioxide, oxides of nitrogen, carbon monoxide, ozone, hydrocarbons, and respirable suspended particles (PM₁₀ and PM_{2.5}). In addition, 24 h averaged PM₁₀ concentrations were obtained from ground-based measurements at sites in North Thailand and Malaysia. The locations of all measurement sites are shown in Figure 3.

3. Methodology

3.1. Case Studies

We investigate three recent cases of transboundary smoke haze in terms of PM₁₀ pollution in Southeast Asia occurring in 2013 and 2014 within two source domains indicated in Figure 3.

3.1.1. Maritime Continent Haze Event

To investigate the severe haze event of June 2013 resulting from fires in central Sumatra, we define the so-called Maritime Continent (MC) domain. The MC domain ranges from 10°S to 19°N and from 94°E to 127°E and encompasses the Indonesian archipelago, the Malay Peninsula, East Malaysia, Brunei, the Philippines, and parts of the Mekong subregion of continental Southeast Asia. The dispersion of smoke haze is simulated from 15 May to 15 July 2013 and compared to hourly- and daily-averaged pollution data from Singapore and Port Dickson, Malaysia.

3.1.2. Thailand Haze Events

Pollution events due to annually recurring fire activity in North Thailand are studied in the boreal springs of 2013 and 2014 in the so-called mainland Southeast Asia (MSA) domain. The MSA domain extends from 4°S to 30°N and from 90°E to 118°E, encompassing parts of the islands of Sumatra and Borneo, the Malay Peninsula, continental Southeast Asia, and Southern China. Simulated smoke haze concentrations are compared to daily-averaged concentration readings from four stations in North Thailand from 6 January to 31 May 2013 and from 6 January to 26 April 2014.

3.2. Emission Characteristics

Fire emissions from GFAS v1.2 are available on a daily basis and used as source data in NAME for each 24 h period from 00 to 24 UTC. In the MSS data set, MODIS fire detections are grouped into 12 h periods from 00 to 12 UTC and 12 to 24 UTC. The 00 to 12 UTC time window includes the two MODIS daytime overpasses (morning and early afternoon, local time) for the region, while the 12 to 24 UTC time window includes two nighttime overpasses. These time groupings allow for the diurnal variation in fire activity to be taken into

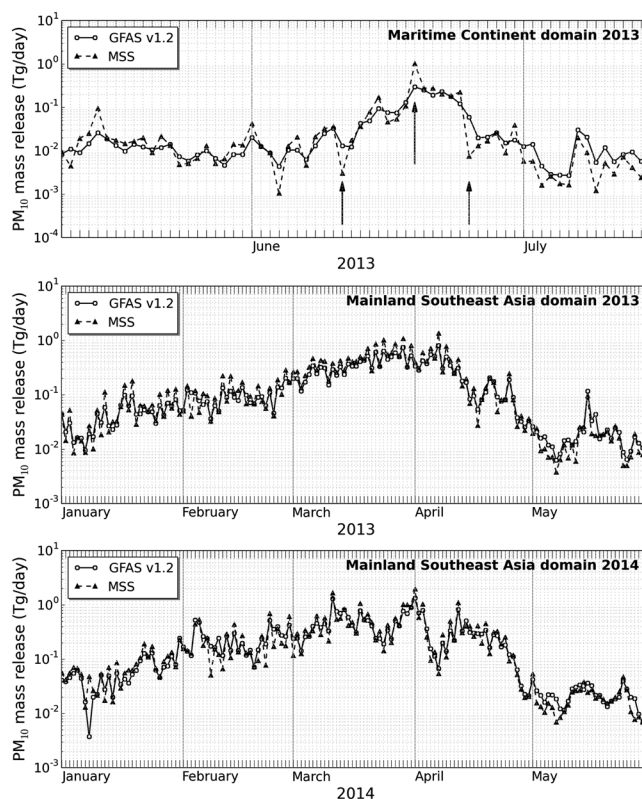


Figure 4. Mass of PM_{10} released per day in the MC domain (top) during the June 2013 haze episode and in the MSA domain during haze events in (middle) 2013 and (bottom) 2014 according to the GFAS v1.2 and MSS emission inventories. Arrows in Figure 4 (top) indicate the 11, 19, and 25 June 2013, approximately corresponding to the onset, peak, and end of the severe pollution recorded in Singapore.

consideration in a basic way. In the dispersion simulations with NAME, the GFAS v1.2 and MSS PM_{10} emission rates are assumed to be constant over their 24 h and 12 h windows, respectively.

Figure 4 shows time series of PM_{10} mass released per day within the entire MC and MSA domains, derived from MSS and GFAS v1.2 data during the three haze events in 2013 and 2014. As both emission products are based on the same underlying MODIS FRP data, there is a high level of qualitative agreement in emission trends. However, the MSS PM_{10} emissions display a significantly higher day-to-day variability. Over some periods of time there is a distinct pattern of MSS exceeding the GFAS emission rates on one day and falling short of them on the other. This is particularly evident in the longer data records for the IC domain in 2013 and 2014. Due to orbital gaps, MODIS fire detections in the tropics display an oscillation with a 2 day period: fire activity is alternately captured well and underestimated the next day [Andela *et al.*, 2013]. This underestimation is compensated for in GFAS by using a persistence algorithm that incorporates previous FRP observations and also includes corrections for cloud cover. Neither of these effects are accounted for in the MSS data set, resulting in the comparatively strong oscillation of source strength amplitudes.

At individual source locations, typically emission rates in the MSS database are higher than in GFAS v1.2, while the daily number of active fire sources in the simulation domains is typically higher in the GFAS data. Pollutant emissions in GFAS v1.2 are produced from the average of MODIS FRP observations available over a 24 h period for each 0.1° grid cell and therefore have a lower magnitude than the direct MODIS FRP observations used in the MSS setup.

3.3. NAME Dispersion Simulations

NAME version 6.3 is used in a parallelized setup for all smoke haze simulations performed in this study. The computational dispersion domains are defined by extending the MC and MSA sources domains described in section 3.1 by 4° (MC domain) and 5° (MSA domain) in meridional and zonal directions. This prevents particles that are released near the edges of the source domains from being lost immediately and allows for some

recirculation of pollutants. The top of the dispersion domain is set to 20 km above ground level to allow dispersion within the tropical troposphere to be fully accounted for.

The NAME runs are performed using time-dependent source location information and corresponding PM_{10} emission rates from GFAS v1.2 and the MSS data sets. Individual wildfire sources are represented as cuboid-shaped releases with horizontal dimensions of $dx = dy = 0.1^\circ$ for GFAS v1.2 and $dx = dy = 0.01^\circ$ for MSS, reflecting the horizontal resolution of each product. The vertical extent of the emissions from the ground, dz , is determined by the injection height described in both data sets with Lagrangian particles being uniformly released within this layer.

For these simulations, NAME was set up to only represent the dispersion and deposition of primary PM_{10} particles that are emitted from wildfire sources. Contributions to the ambient PM_{10} levels from other natural or anthropogenic (e.g., industry and traffic) sources and from secondary aerosol formation are not accounted for. Hence, output model concentrations consistently lack a background pollution level. The modeled PM_{10} particles are subject to wet and dry deposition mechanisms.

In order to ensure an acceptable level of statistical noise in the output from the Lagrangian dispersion simulations, we set up the model to release large numbers of particles for each source location (100 and 50 per hour for the MC and MSA case studies, respectively). Depending on the overall number of fire sources, the average number of computational particles present in the domains over 1 h of simulated time was in the range of approximately 0.5–50 million. The maximum travel time of each particle is set to 96 h for the benefit of computational efficiency. After this time it is reasonable to assume that most particles will have left the domain and those that have not will have traveled a significant distance away from the source so are well dispersed and have been affected by deposition processes, contributing to comparatively low concentration levels. A spin-up time of a minimum of 4 days is implemented in all runs in order to create realistic initial PM_{10} levels resulting from biomass burning prior to retrieving the first model output.

Concentration outputs in terms of local time series at specific locations and spatial plumes are retrieved as hourly and daily time averages. PM_{10} time series are extracted within NAME by specifying output grid boxes centered on the location of the air quality monitoring sites. A horizontal grid box resolution of $dx = dy = 0.1^\circ$ has been found to provide adequate statistical noise reduction in the retrieved model outputs. Concentrations are furthermore represented as boundary layer averages using depth information available from the driving NWP model.

3.3.1. Meteorological Data

The global configuration of the Met Office Unified Model (MetUM) [Davies *et al.*, 2005] was used to supply three-dimensional deterministic input meteorology to NAME. The MetUM can be used in different configurations across varying time and space scales (e.g., for short-range weather forecasting, seasonal forecasting, and climate predictions). The atmospheric component of the model uses nonhydrostatic dynamics. Subgrid-scale processes represented include convection, boundary layer turbulence, radiation, cloud microphysics, and orographic drag.

MetUM uses a hybrid ensemble 4 day variational data assimilation system to assimilate available observations into the model initial state. Forecasts are produced on a 6 h cycle to produce four forecast runs per day. Model fields are output for NAME at a temporal resolution of 3 h. The operational configuration of the global forecast model during the period for this study supplied meteorological fields with a horizontal resolution of 0.35° (longitude) by 0.23° (latitude), and with 70 nonuniform vertical levels extending to an altitude of 80 km. Meteorology in NAME for the haze simulation setup extends to an altitude of 20 km, using the lowest 53 MetUM model levels. Within NAME, meteorological data are interpolated in both space and time.

The NAME simulation will be influenced by uncertainties in the meteorological modeling in the MetUM and in the transport and dispersion processes within NAME and by uncertainties associated with source characteristics (e.g., release amount, height, and location). These uncertainties, which are not examined directly here, would include aspects such as exchange at the top of the boundary layer (BL), which requires an accurate estimate of BL depth from the NWP, vertical transport by moist convection, and pollutant washout by rainfall. The use of strongly unphysical NWP BL depth values in NAME is avoided by setting the minimum/maximum BL depths allowed in the dispersion simulations to 80 m and 4 km, respectively.

4. Results

In the following we validate NAME haze simulations for MSA and the MC against ground-based PM_{10} measurements. For each pollution scenario we determine correction factors for local model concentrations by means of a regression analysis over the entire pollution episode. Based on the Singapore haze event of 2013 we also explore the potential of using a more flexible bias correction approach, which can be used in real time to account for systematic errors in the emissions and modeling.

4.1. June 2013 Case Study

We evaluate Lagrangian dispersion simulations of the June 2013 haze episode within the MC domain by means of comparisons with PM_{10} observations from the dense air quality monitoring network in Singapore and from a measurement site at Port Dickson, Malaysia (Figure 3). In the case of Singapore, this is achieved by comparing concentrations that are spatially averaged over all the measurement sites.

Since our simulations only account for PM_{10} released from wildfires, background pollution levels are systematically missing from the model results. In order to allow for a direct comparison with the observations, we determined approximate background PM_{10} concentrations for each comparison site and corrected the simulation results accordingly. Based on daily-averaged PM_{10} levels from all 12 measurement sites in Singapore, we determined an approximate mean background pollution of $30 \mu\text{g}/\text{m}^3$ with a standard deviation of $8 \mu\text{g}/\text{m}^3$ during haze-free periods from 1 January 2013 to 26 April 2014. The analyzed data included comparatively “clean” periods in terms of pollution from natural or anthropogenic sources other than biomass burning, but also periods of significant background pollution levels, with a range (i.e., maximum minus minimum pollution levels) of $52 \mu\text{g}/\text{m}^3$ detected over the analysis period. These ranges and average values are in agreement with PM_{10} levels reported by *Chew et al.* [2013] over an analysis period from September 2009 to March 2011. Background PM_{10} levels at Port Dickson, Malaysia, were found to be higher with an approximate mean background level of $38 \mu\text{g}/\text{m}^3$, a standard deviation of $\pm 9 \mu\text{g}/\text{m}^3$ and a value range of $53 \mu\text{g}/\text{m}^3$ for haze-free periods from 1 January 2013 to 31 December 2013.

Using a linear regression analysis as a postprocessing step, we estimate approximate scaling factors for the NAME-GFAS and NAME-MSS outputs that are required to match the concentration levels observed and taking into account the estimated baseline PM_{10} pollution levels (for details, see supporting information for this article). For Singapore we obtained scaling factors of 1.9 for NAME-GFAS and 0.9 for NAME-MSS, while at Port Dickson scaling factors of 2.3 (GFAS v1.2) and 0.7 (MSS) were determined. It has to be noted that the MSS correction factor for Port Dickson would have been higher (on the order of 1.5) if the scaling had been specifically targeted at matching the peak concentrations instead of using a more “global” approach via a regression analysis. This scaling behavior is not mimicked in the results from the GFAS setup.

Scaled model results from NAME-GFAS and NAME-MSS for Singapore are shown in Figure 5 together with corresponding daily and hourly-averaged PM_{10} measurements. For Singapore, modeled and observed concentrations represent averages over all 12 monitoring stations. Also shown are daily PM_{10} averages at the air quality monitoring site in Port Dickson.

A high level of temporal correlation between simulations and observations in Singapore is evident over the peak pollution period. However, both simulations feature an overall shorter duration of the haze event, not capturing the onset of the episode around 15 June and failing to reproduce the elongated tail present in the observations from 26 June to 1 July. This is particularly pronounced for NAME-MSS, which only indicates very high pollution levels in a narrow window around 20 June. NAME-GFAS better reproduces the short-term variability seen in the hourly observations during the peak period between 16 and 24 June. At Port Dickson, a distinct three-peak pattern is evident in observations and simulations, but with the latter not quite matching the timings observed in the field. In NAME-MSS a rapid decline of PM_{10} concentrations takes place on 24 June, resulting in a significantly reduced length of the event compared to the observations and NAME-GFAS.

These findings are in agreement with the differences evident in the PM_{10} mass release within the MC domain shown in Figure 4. The MSS emissions are significantly lower compared to GFAS v1.2 at the beginning (11 June) and end (25 June) of the haze event, but much higher during the peak period (19 June). The high concentration of fires in the Riau Province in Sumatra led to a sharp increase in the number of hot spots represented in the MSS data set due to the higher spatial resolution used. Since mainly peat was burning in Riau [*Gaveau et al.*, 2014], the accuracy with which peat is represented is crucial. The fraction of peat in the land cover maps used to derive the GFAS v1.2 emissions is much smaller compared to the MSS data set (Figure 2), offering

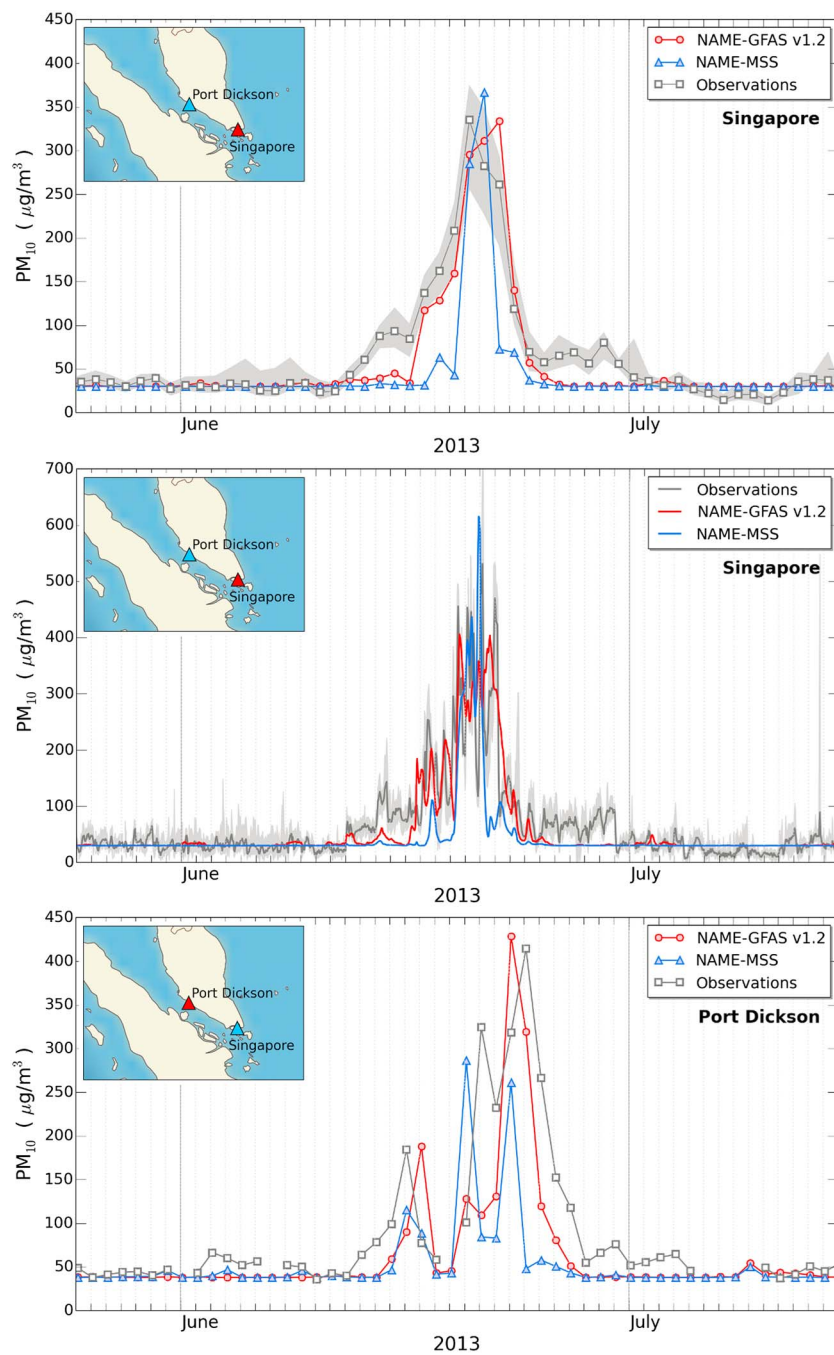


Figure 5. Scaled NAME-GFAS and NAME-MSS results for the June 2013 haze episode together with (top) daily PM_{10} averages from Singapore, (middle) 1 h averaged PM_{10} observations from Singapore, and (bottom) daily observations from Port Dickson, Malaysia. Grey areas in the Singapore records indicate the range of concentrations detected over all 12 measurements sites. Simulation results are presented as boundary layer averages.

an explanation for the higher smoke emissions observed in the latter during the peak of the event and for the differences in scaling factors determined for NAME-GFAS and NAME-MSS. The significantly lower release strengths at the onset and end of the event are believed to be linked to the increased cloud fractions over central Sumatra as visible in Terra/Aqua satellite images. Cloud cover effects are particularly evident in the MSS data set where fire persistence and cloud cover correction algorithms are not applied.

For a more quantitative comparison between the scaled model results and the field observations, different validation metrics are displayed in Table 2a and introduced in more detail in Appendix A. For Singapore and

Table 2. Validation Metrics for Bias-Corrected NAME-GFAS and NAME-MSS Simulations: (a, b) Bias Correction Using Scaling Factors Derived for Each Site Via a Regression Analysis Based on Hourly (Singapore) and Daily Concentration Observations (Port Dickson; North Thailand); (c) Real-Time Bias Correction Using an Additive 24 h Median Bias for the June 2013 Haze Episode Together With Metrics From Persistence Tests

| | | | FAC2 | | MNMB | | FGE | | R | |
|-----|------|--------------------|-----------|----------|-----------|----------|-----------|----------|-----------|----------|
| | | | NAME-GFAS | NAME-MSS | NAME-GFAS | NAME-MSS | NAME-GFAS | NAME-MSS | NAME-GFAS | NAME-MSS |
| (a) | 2013 | Singapore | 0.84 | 0.75 | -0.05 | -0.17 | 0.36 | 0.43 | 0.86 | 0.68 |
| | | Port Dickson | 0.87 | 0.83 | -0.26 | -0.34 | 0.34 | 0.38 | 0.81 | 0.45 |
| (b) | 2013 | Chiang Mai | 0.95 | 0.92 | -0.2 | -0.26 | 0.26 | 0.33 | 0.89 | 0.89 |
| | | Chiang Rai | 0.84 | 0.82 | -0.24 | -0.29 | 0.32 | 0.38 | 0.84 | 0.78 |
| | | Mae Hong Son | 0.79 | 0.62 | -0.38 | -0.48 | 0.44 | 0.55 | 0.8 | 0.74 |
| | | Lampang | 0.94 | 0.89 | -0.01 | -0.13 | 0.25 | 0.34 | 0.78 | 0.62 |
| | 2014 | Chiang Mai | 0.71 | 0.65 | -0.37 | -0.58 | 0.46 | 0.66 | 0.7 | 0.4 |
| | | Chiang Rai | 1.0 | 1.0 | -0.15 | -0.13 | 0.21 | 0.22 | 0.91 | 0.87 |
| | | Mae Hong Son | 0.74 | 0.71 | -0.39 | -0.3 | 0.43 | 0.44 | 0.75 | 0.75 |
| | | Lampang | 1.0 | 0.9 | -0.09 | -0.19 | 0.25 | 0.32 | 0.63 | 0.39 |
| (c) | 2013 | Singapore | 0.92 | 0.88 | 0.01 | 0.004 | 0.31 | 0.33 | 0.87 | 0.73 |
| | | persistence actual | | 0.83 | | 0.0002 | | 0.37 | | 0.78 |
| | | persistence median | | 0.88 | | 0.023 | | 0.33 | | 0.81 |

Port Dickson, the majority of scaled model results are well within a factor of 2 (FAC2) of the observations, but the modified normalized mean bias (MNMB) shows that both models are systematically underpredicting. The overall simulation error, measured by the fractional gross error (FGE), is slightly lower for NAME-GFAS. The correlation coefficient (R), which is independent of the introduced quantitative scaling, indicates a high level of qualitative agreement between NAME-GFAS and temporal patterns evident in the local PM_{10} observations. Hence, the metrics quantitatively reflect the fact that NAME-GFAS provides a better representation of the short time variability of smoke haze pollution for this event together with a closer match in terms of the overall duration.

4.1.1. Smoke Haze Plume Behavior

Analyzing spatial dispersion patterns of haze plumes is essential to better understand causes for the discrepancies observed in the local concentration time series. Figure 6 shows unscaled PM_{10} concentration plumes from NAME-GFAS during the onset, peak, and decline of the severe smoke emissions from central Sumatra. Despite the fact that local concentration levels differ, the plume envelopes and overall dispersion behavior are very similar to NAME-MSS (not shown). Concentrations shown are 24 h averages valid at 00 UTC and therefore are based on emission information available during the preceding day from 00 to 24 UTC. The plumes represent boundary layer averaged concentration fields based on BL depths diagnosed by the MetUM. Figure 7 shows corresponding MetUM early afternoon wind fields at a height of 1 km together with precipitation rates. The wind fields are plotted over GFAS v1.2 emission rates from fire hot spots that were active during the 24 h period covering that day.

At the onset of the haze episode around 15 June, the MetUM shows very light southerly winds over the hot spot area in central Sumatra but a quite strong westerly flow farther north and over the Malay Peninsula. During this phase, pollutant plumes from Sumatra are transported in a northeasterly direction, with the high-concentration center of the plume lying north of Singapore, resulting in the first pollution peak at Port Dickson (Figure 5). Both NAME-GFAS and NAME-MSS underpredict the concentration levels during the early phase of the event. This may be attributed to a too strong southerly flow component in the MetUM. During the peak period of fire activity around 20 June, emissions are transported straight across the Strait of Malacca into Malaysia and Singapore by strong westerly winds that are enhanced by the presence of a tropical cyclone in the South China Sea. The downwind edge of the smoke plume reaches as far as the Philippines.

Dry weather conditions persisted into the second half of June and the fire activity in Sumatra continued to be very intense (Figure 4). However, as the tropical cyclone made landfall, the low-level winds over Singapore shifted to a south-southeasterly direction, locally resulting in a strong improvement of the pollution situation compared to the preceding days (see also Figure 5). With the plume moving northward, the haze situation in

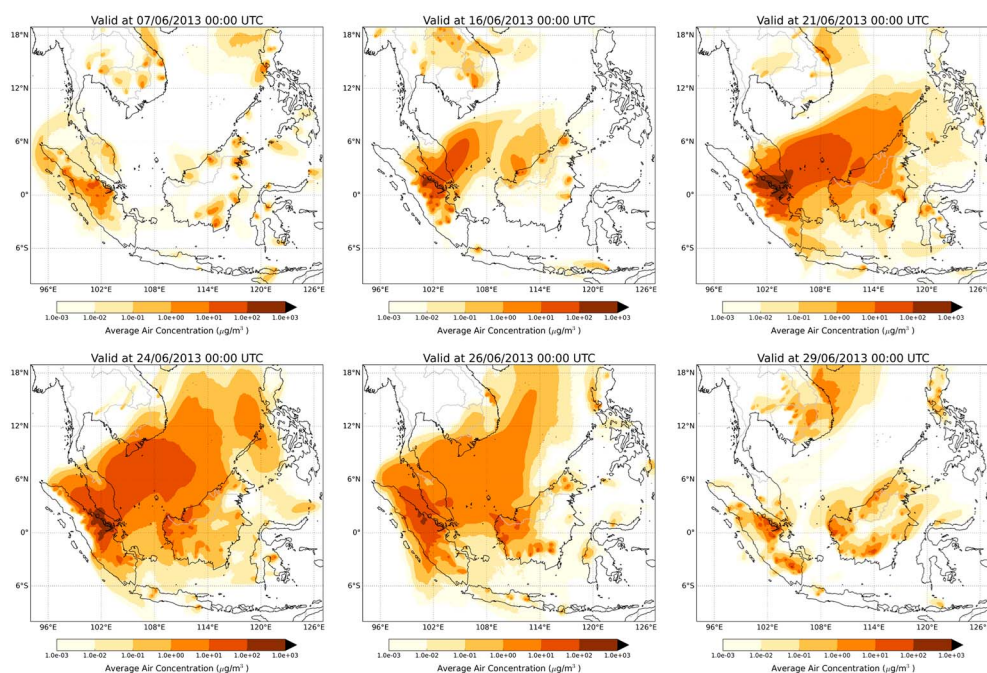


Figure 6. 24 h averaged NAME-GFAS PM_{10} concentrations within the boundary layer (not bias corrected) during the onset, peak, and end of the June 2013 smoke haze episode in the Maritime Continent.

Port Dickson reached its worst state around 24 June. At the same time, convective activity in the entire region picked up, resulting in rainfall over the Sumatran hot spot area. This put an end to the anomalous dry spell that had prevailed over Riau Province for about two months [Gaveau *et al.*, 2014]. The rain quickly helped to subdue most of the fires in Sumatra, resulting in a significant improvement of the haze situation in the entire region during the last days of June. Very light and variable winds confined the remaining smoke haze close to the fire sources (Figure 6).

The increased cloud cover over the area is likely to have significantly contributed to the differences between NAME and local observations (Figure 5). While increased precipitation leads to a fast but gradual decrease of fire activity in the area, the FRP retrievals suggest a more-or-less instantaneous shut-off of emissions. While partial cloud cover is accounted for to some degree in the generation process of the GFAS v1.2 emissions, there is a limit to the correction scheme when multipixel areas are obscured by persistent cloud cover. Very light and variable winds at the end of June also resulted in haze-obscuring fire hot spots, contributing to further emission underestimations. It is also likely that smoldering fires were still actively emitting significant amounts of pollutants even after the rain set in, particularly so in peat areas. FRP signals associated with these low-intensity fires may not have been detected by the MODIS instruments, resulting in an undersampling of hot spots.

4.2. Thailand Case Studies

Severe air pollution due to smoke haze from crop-residue burning and land conversion and forest fires affects continental Southeast Asia every year in the months prior to the onset of the Indian monsoon in May. Strongly stable layers and temperature inversions quite frequently can be observed in the region [Nodzu *et al.*, 2006, 2011], trapping wildfire emissions in the lower troposphere. Multiyear spaceborne lidar measurements analyzed by Gautam *et al.* [2013], for example, showed evidence that aerosols are mostly concentrated within the boundary layer.

We simulate haze episodes in 2013 and 2014 with NAME-GFAS and NAME-MSS and validate the results against ground-based observations of PM_{10} (24 h averages) from four measurement sites in the North Thailand provinces of Chiang Mai, Chiang Rai, Mae Hong Son, and Lampang (Figure 3). For this region, the study by Gautam *et al.* [2013] using data from the AERONET project found particularly high smoke haze aerosol loadings (Chiang Mai) during the annually recurring haze season.

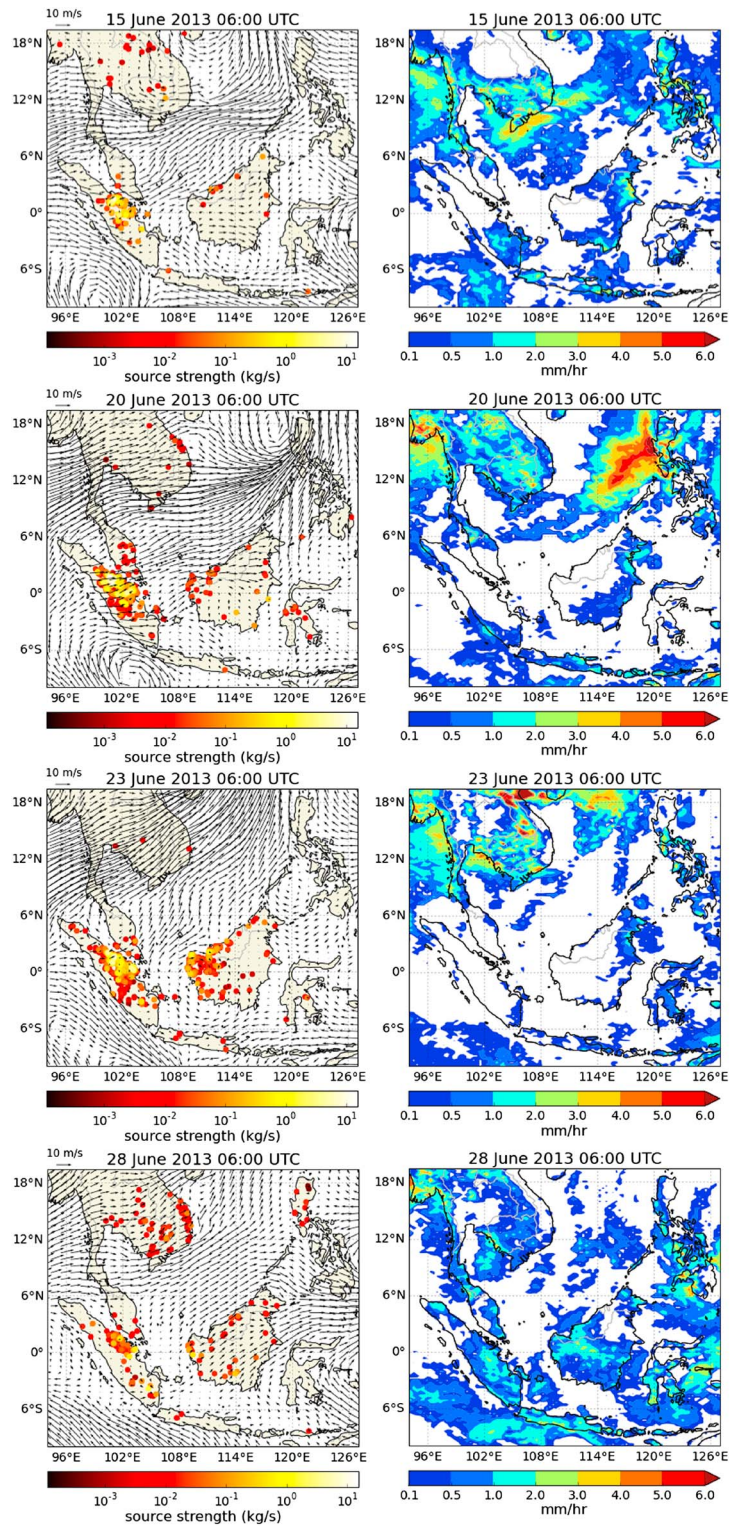


Figure 7. MetUM early afternoon local time (left column) 1 km wind fields and (right column) precipitation rates during the June 2013 haze episode. Wind vectors are plotted over GFAS v1.2 PM₁₀ emission rates from wildfire sources that were active from 00 to 24 UTC.

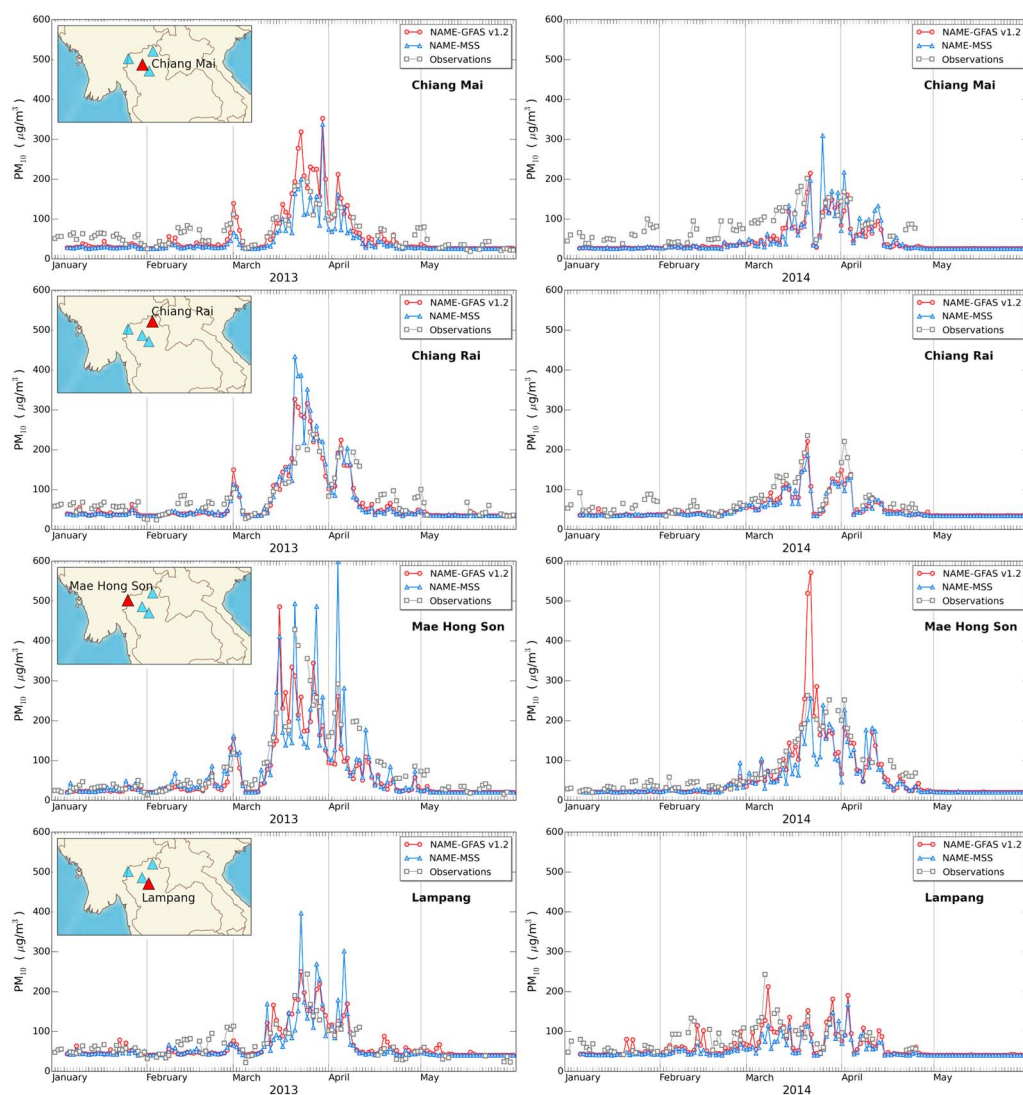


Figure 8. Same as Figure 5 but for the mainland Southeast Asia smoke haze episodes in 2013 (left column) and 2014 (right column) detected at four sites in North Thailand. Modeled and observed PM_{10} concentrations represent daily averages.

Nonhaze background levels of PM_{10} observed at the four sites in North Thailand during the period of 1 May 2013 to 31 December 2013 are the following: Chiang Mai: average of $26 \mu\text{g}/\text{m}^3$ with a standard deviation of $\pm 13 \mu\text{g}/\text{m}^3$ and a data range of $70 \mu\text{g}/\text{m}^3$; Chiang Rai: $34 \mu\text{g}/\text{m}^3 \pm 19 \mu\text{g}/\text{m}^3$ (range: $106 \mu\text{g}/\text{m}^3$); Mae Hong Son: $21 \mu\text{g}/\text{m}^3 \pm 12 \mu\text{g}/\text{m}^3$ (range: $68 \mu\text{g}/\text{m}^3$); Lampang: $41 \mu\text{g}/\text{m}^3 \pm 16 \mu\text{g}/\text{m}^3$ (range: $84 \mu\text{g}/\text{m}^3$).

For each of the four sites we calculated scaling factors based on the 2 month high-pollution period in March and April of 2013 and 2014 via a regression analysis. For the 2013 haze episode, the site-specific scaling factors for the NAME-GFAS simulation varied between 3.9 and 5.6, while for NAME-MSS scaling factors ranging between 4.0 and 6.7 were obtained. For the 2014 pollution event, the quantitative differences between NAME-MSS and local PM_{10} observations showed a stronger site-to-site variability with scaling factors ranging between 3.4 and 8.1. For the same period of time, site-specific scaling factors for NAME-GFAS showed a slightly smaller range from 4.6 to 5.6 compared to 2013.

The correspondingly scaled and background pollution-corrected NAME-GFAS and NAME-MSS simulations are shown in Figure 8 together with observations. Table 2b displays quantitative validation metrics for both events. With few exceptions, there is a high level of correlation between the measured and simulated local concentration levels during the periods of significant pollution in March and April. Scaling the raw model

output results in negative normalized biases and FGE values that are comparable to the metrics obtained for the June 2013 haze episode. Compared to the haze event in maritime Southeast Asia, however, qualitatively the results of NAME-GFAS and NAME-MSS are more consistent with each other. Differences observed between NAME-GFAS and NAME-MSS are believed to be mainly attributable to differences in conversion and emission factors used (all for nonpeat land types) as well as to the way in which the loss of FRP information due to obscuration by cloud and haze is treated.

Differences in the magnitude of the scaling factors for the North Thailand sites compared to Singapore and Port Dickson mainly reflect differences in regional source characteristics and fire types (i.e., different land use/cover characteristics and resulting differences in fire fuel types; absence of peat). Year-to-year differences in scaling factors for the same region, as encountered for the Thailand haze events, also indicate a variability in local fire characteristics in connection with meteorological pattern prevailing during the analysis period and the associated predictive skill of the NWP model.

4.3. Real-Time Bias Correction

With the above analyses we were able to establish confidence in using the Lagrangian dispersion modeling approach combined with emission estimates derived from active-fire detections to qualitatively capture local haze pollution levels in Southeast Asia. However, the analyses also showed that it is necessary to apply some scaling to the model results in order to arrive at a quantitative agreement with locally observed pollutant concentrations. The scaling factors derived here are similar in magnitude to the factors reported by *Hyer and Chew* [2010], who used the Eulerian model NAAPS together with FLAMBE to analyze a Maritime Continent haze event occurring in 2006 and also evaluated their model results against ground-based air quality observations in Singapore and Malaysia. Our analysis showed that the scaling factors strongly depend on the region of interest, due to differences in local land cover characteristics, fire fuel types, and prevailing meteorological conditions. In the case of North Thailand, we also observed a time dependency from one year to the other. Hence, it cannot be expected that the scaling factors will be equally valid for future haze events. For the setup of an operational quantitative smoke haze forecast a more flexible scaling scheme needs to be used.

We revisit the June 2013 haze episode and apply a bias correction scheme to hourly PM₁₀ model time series for Singapore. Real-time bias correction based on observations can be used to improve operational air quality and pollutant dispersion forecasts [e.g., *Borrego et al.*, 2011; *Neal et al.*, 2014]. Systematic and random model errors introduced, for example, by regionally varying uncertainties in emissions or NWP skill can be addressed through such a correction process. Applying bias correction to the model output as a postprocessing step is a pragmatic approach for optimizing the prediction of localized near-surface concentrations based on available real-time observations. The methodology, however, does not attempt to adjust the original emission terms (or, equivalently, the overall smoke budget).

We explore the practicality of using real-time bias correction based on surface observations in Singapore for the operational smoke haze forecast demonstration system presented here. Following the hybrid forecast technique described by *Kang et al.* [2008], we correct raw model outputs of PM₁₀ concentrations at a certain monitoring site using a residual determined from observations and model results for that site at previous times. With this approach we are assuming a short-term persistence of the model bias at each site. In our study, the corrected concentration forecast at site *i* is obtained according to

$$M_{i,t+j}^{\text{corr}} = M_{i,t+j} - \tilde{b}_{i,t}, \quad (1)$$

where $M_{i,t+j}$ is the raw forecast issued at time t for $j = 0, 1, \dots$ hours lead time and

$$\tilde{b}_{i,t} = \text{median} [(m_{i,t-N} - o_{i,t-N}), \dots, (m_{i,t} - o_{i,t})] \quad (2)$$

is the sample median of $N + 1$ residuals computed between raw forecasts, m , and observations, o , at site i prior to the forecast issue time t . From sensitivity tests carried out on the basis of hourly-averaged concentration observations in Singapore, we determined an optimum analysis window of 24 h prior to the forecast issue time to determine a representative residual according to equation (2). Using the median assures that occasional outliers in the sample of hourly residuals do not affect the robustness of the retrieved statistic.

In order to create a resemblance to a real-life forecast product, the NAME-GFAS and NAME-MSS simulation outputs are split up into 24 h concentration forecast blocks (i.e., corresponding to daily forecasts with

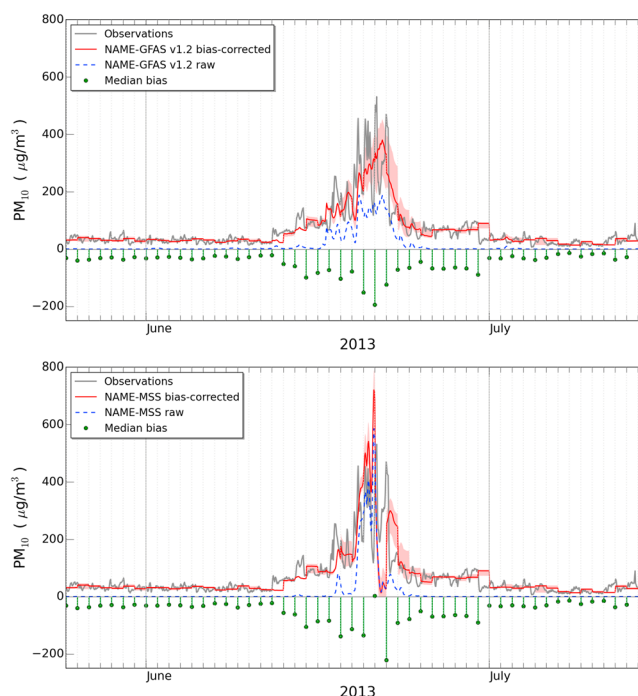


Figure 9. Bias-corrected (top) NAME-GFAS and (bottom) NAME-MSS simulations of the June 2013 haze episode in Singapore based on the median bias determined over a 24 h analysis window. Hourly simulation and observation data represent averages over all 12 local monitoring sites in Singapore. Red areas indicate the forecast margins based on the 25th and 75th bias quantiles.

24 h maximum lead time and hourly output). Figure 9 shows concatenated time series of the bias-corrected daily NAME forecasts for Singapore based on the median bias determined over a 24 h analysis window. Both the simulation and observation data represent averages over all 12 local monitoring sites in Singapore. The median bias is assumed to persist over the entire 24 h forecast length. For both NAME-GFAS and NAME-MSS the bias correction resulted in a much better representation of the early phases and declining stages of the haze episode. A similar level of agreement during the peak period is evident when comparing the new results using the additive bias to the earlier scaling approach (see Figure 5, middle). Step-like patterns in the NAME concentration signals occur whenever the raw model output is zero, indicating that no PM_{10} pollution from wildfire sources arrived at the monitoring sites. The bias correction approach automatically accounts for background PM_{10} levels, which is beneficial from an operational point of view since industrial or traffic pollution can vary quite strongly on short time scales. Short-term variations of nonfire-related anthropogenic or natural pollution during the course of the forecast period, however, cannot be predicted with this system as NAME is not being run as an air quality model. Influences of such short-term fluctuations on the predictive skill of the model would need to be assessed based on evidence from other air quality measurements.

Table 2c shows updated validation metrics based on the new bias correction scheme. Compared to the regression-scaling approach (Table 2a) the more flexible bias correction resulted in an improvement of all metrics, particularly so for the NAME-MSS simulations. Also shown here are metrics determined from persistence tests using only the observations from the Singapore air quality network. The metrics were determined by (1) persisting the entire observation time series (averaged over all sites) from the previous day into the future for 24 h on an hour-by-hour basis (persistence actual) and by (2) persisting only the median PM_{10} level that was determined from the observations during the previous day (persistence median). Comparing the metrics from the persistence test with the metrics determined for the bias-corrected NAME simulations shows a significantly improved simulation skill for NAME-GFAS. Here the very small value of MNMB for the persistence-actual method does not reflect a higher skill, but rather a random cancelation of overpredictions and underpredictions, which is known to affect the representativeness of this metric. The NAME-MSS skill, on the other hand, is comparable to the persistence test based on the median of previous day observations in terms of FAC2 and FGE and reduced when looking at the correlation coefficient.

This result is linked to the raw NAME-MSS simulation showing an overall reduced duration of the haze event compared to NAME-GFAS. Whenever the raw model output shows zero concentrations from biomass burning at the location of interest, the bias correction approach will result in a forecast that is purely based on a persistence of the median (equation (1)). However, if the model delivers a better representation of the local temporal evolution of smoke haze pollution, as seen in NAME-GFAS, the bias correction approach clearly outperforms the persistence test.

5. Discussion and Conclusions

We have investigated smoke haze pollution episodes in maritime and continental Southeast Asia by running the Lagrangian particle model NAME with two biomass-burning emission inventories based on active fire detection by MODIS instruments. Our results show that the extreme haze conditions observed in the Maritime Continent and in mainland Southeast Asia in 2013 and 2014 can be reproduced by this modeling system. Both GFAS v1.2 and MSS emission repositories represent the temporal variation of fire intensities in the area very well. Combining these sources with the Lagrangian dispersion modeling approach using meteorological fields from the MetUM resulted in a high level of qualitative agreement with ground-based pollution measurements. However, in order to arrive at an acceptable quantitative match of concentration magnitudes, it was necessary to introduce a scaling/bias correction to the raw model output.

Shortcomings in the reproduction of locally observed pollution magnitudes and the qualitative and quantitative differences between NAME-GFAS and NAME-MSS are linked to complexities involved in the modeling of biomass burning emissions. Dominant contributing factors are the following:

Land Cover Information. Accurate information about fuel types plays a crucial role for estimating pollutant fluxes, particularly when high-emission fuels like peat are present in the fire area [e.g., Hyer and Chew, 2010]. There is a recognized need to reduce uncertainties in source emissions, especially for a quantitative operational forecast system outputting hourly predictions of PM_{10} . The modeling comparison of different fire emission inventories by Zhang *et al.* [2014] showed that the reliability of simulations of atmospheric aerosol loading and transport is highly influenced by emission uncertainties, with the largest influence at local and hourly-to-daily scales.

The fact that the MSS approach uses a significantly more detailed representation of peat areas in the eastern part of central Sumatra than GFAS v1.2 is believed to have contributed strongly to the differences seen between the NAME simulations of the June 2013 haze event. While the NAME-GFAS raw output underpredicted concentrations by approximately a factor of 2, the raw NAME-MSS results matched the observed peak levels of PM_{10} in Singapore and Port Dickson considerably better. This result underlines the importance of an accurate representation of peat in the Maritime Continent. In agreement with that, biomass burning in nonpeat, highland areas of mainland Southeast Asia resulted in a higher level of congruence between NAME-MSS and NAME-GFAS. Differences can be further attributed to the fact that the MSS emissions are derived with updated emission and conversion factors in combination with more recent, better-resolved land cover maps. Keeping track of the rapid land conversions taking place in parts of Southeast Asia and updating land-class maps correspondingly is crucial to deliver reliable emission products.

Representation of Fire Activity. Another important factor contributing to the observed differences between NAME-GFAS and NAME-MSS is related to the way in which missing FRP observations are treated. The fact that GFAS v1.2 corrects for partial hot spot obstructions due to cloud and/or smoke haze while the MSS approach does not, significantly contributed to differences in the persistence of local pollution levels observed during the June 2013 haze event. On the other hand, continuous cloud cover that is often encountered in terms of ubiquitous cirrus in Southeast Asia [e.g., Reid *et al.*, 2013] can make it very difficult to derive accurate information about fire activity from space. Another general issue is presented by detection limitations of the MODIS instruments regarding fire pixels of low radiative intensity. Wooster *et al.* [2003] show that MODIS can underestimate the FRP of low-intensity fires by up to 46% when compared to measurements from the Bi-spectral InfraRed Detection (BIRD) small satellite, which is equipped with dedicated sensors for active fire detection. Low-intensity, smouldering fires can result in significant emissions depending on their number and on the particular fuel (e.g., peat).

Injection Heights. While GFAS v1.2 uses a plume-rise model to estimate the initial injection height of pollutants, resulting in local emission depths varying between a few decameters to a few kilometers above

ground, MSS uses a fixed height of 800 m. We performed a sensitivity test for the Maritime Continent haze event by fixing the injection height in GFAS v1.2 to 800 m and comparing the results to the original NAME-GFAS run in Singapore. Particularly during the peak of the event, fixing the injection height resulted in significantly reduced local concentration levels and increased model differences with the observations (not shown). The majority of GFAS sources are associated with injection heights that are significantly lower than 800 m. Pollutants are therefore primarily emitted directly into the lower portions of the atmospheric boundary layer. Representing these vertically confined emissions in Sumatra proved to be important for a better reproduction of ground-level concentrations in Singapore. Regarding the MSS emissions, it has to be investigated whether site-specific injection heights retrieved from a plume-rise model would consequently result in an overprediction of PM_{10} levels for the June 2013 scenario.

Background Pollution. The NAME dispersion simulations are purely driven by emissions from biomass burning. Hence, the forecast will constantly lack local baseline pollution levels associated with other natural or anthropogenic sources of particulate matter (e.g., due to sea salt, dust, industrial, or traffic emissions). The impact of such local or regional sources on near-surface air quality in Singapore can vary on a range of different time and geographic scales. The real-time bias correction approach presented here takes into account the local background pollution based on observations from the past 24 h, which are then projected into the forecast period. The skill of the bias-corrected haze prediction, however, can of course be further influenced by short-term changes of anthropogenic emissions taking place during the forecast period. While for the large event in June 2013 short-term fluctuations of other local/regional pollutant sources are deemed to have a minor overall effect on the skill of the simulation, particularly in comparison to uncertainties in the emission inventories, this may not be true for future haze episodes. Forecasts and observations for other pollutants like $PM_{2.5}$ can be of help in assessing the impact of anthropogenic emissions on local air quality in relation to smoke haze from biomass burning (see also section 5.1). Furthermore, taking into account the information from a multitude of sites, as done in the case of Singapore, helps to mitigate effects of strong spatial variability of background pollution levels within the domain of interest.

The accuracy of dispersion simulations with Lagrangian particle models like NAME to a large degree depends on the accuracy of the driving meteorological data. Given the moderate resolution of the global configuration of the MetUM, coastal regions and smaller islands, including Singapore, are not reproduced in detail or, in some cases, not at all. Not fully representing the complex distribution of land, sea and terrain in the Maritime Continent has to be expected to have an influence on local dispersion features, for example, by missing important local flow features induced, for example, through the presence of orographic features and/or land-sea contrasts. *Milton et al.* [2015] discussed that the MetUM, in common with other global NWP models, suffers from systematic errors affecting the representation of multiscale convection and associated diurnal cycles in Southeast Asia, particularly over land. Inaccuracies in precipitation rates and rainfall locations can feed back to the dispersion simulation in terms of erroneous wet deposition rates of pollutants. The accuracy of low-level wind fields is adversely affected by errors in the representation of moist processes and diabatic heating and is also influenced by "remote errors" from other regions, e.g., through monsoon forcing errors [*Milton et al.*, 2015].

The quantitative bias detected in local NAME concentration outputs needs to be addressed in a flexible way in order to account for the interaction of different factors influencing the simulation skill. Inaccurate estimates of emission rates and source locations are believed to be dominant contributors to quantitative discrepancies detected between simulations and observations. However, inaccuracies in other parts of the modeling system, for example, the NWP or dispersion model, play a role as well. We have presented an approach to address the combined forecast bias in a more flexible way by using a real-time bias correction technique that can be implemented into a quantitative operational haze-forecast system. The approach automatically corrects for background concentration levels that cannot be attributed to biomass burning and whose explicit inclusion would add considerably to the forecast system complexity and computational costs. Furthermore, the technique will not be affected by internal changes to parts of the modeling system, for example, regarding the emission inventories (e.g., updates to conversion/emission factors, correction schemes, or plume-rise information). When using GFAS or MSS emission products in operational forecasts, it needs to be considered that the evolution of fire activity and corresponding emissions over the duration of the forecast is unknown. Persisting fire emissions that are valid at the initiation of the forecast into the future can be used as a first guess but inevitably will introduce errors. Since air quality observations are also needed in near real time, it also has to be taken into account that these measurements have not yet been fully quality controlled by the

time they are introduced into the bias correction system. Receiving information from a network of sensors as in the example of Singapore can help to mitigate this problem.

5.1. Conclusions and Outlook

Poor air quality due to smoke haze pollution continues to be a major problem in Southeast Asia, affecting the health of millions of people in the region on short and long time scales. Following a dry spell in early March 2014 fire intensities in the Riau Province in Sumatra again reached levels comparable to the June 2013 event. On this occasion the severe haze mainly affected central Sumatra as the smoke was transported toward the Indian Ocean by prevailing northeasterly winds.

Thus, it is an urgent task to introduce regional air quality forecasts targeted at the prediction of such smoke haze pollution events. The near real-time availability of biomass-burning emission products based on MODIS active-fire detection shows strong potential for the applicability within an operational haze-forecast system. Our case studies based on high temporal and spatial resolution dispersion simulations with NAME combined with a flexible bias correction scheme targeted at Singapore can be successfully applied to improve the simulation accuracy of local pollution levels.

Next steps will concentrate on exploring the skill of bias-corrected smoke haze predictions with NAME-GFAS and NAME-MSS for Singapore in an operational environment based on events occurring since mid-2014. In an operational setup, the modeling system takes between 2 and 3 h to produce a forecast, consisting of a 4 day spin-up followed by a 48 h forecast period, depending on the number of fires in the region. These timings are from tests on a single server and would be significantly faster on a high-performance computer.

In the next steps of the work, particular attention will be directed at investigating the skill of the forecasts with increasing lead time. Another focus will be on exploring bias correction approaches of NAME concentration plumes by making use of ground-based observations available in the wider region. Information about the vertical structure of aerosols in the atmosphere, such as AOD measurements from satellites and LIDAR, will also be assimilated into the system. Forecast accuracy gains from running on high-resolution meteorological data from limited-area NWP models will also be investigated. Observations $PM_{2.5}$ will be used to further investigate the forecast skill of the modeling system in future haze events. $PM_{2.5}$ observations may also prove helpful to disentangle uncertainties associated with the smoke haze modeling system from short-term fluctuations of local baseline pollution levels.

Our analyses showed that detailed information about fuel types, particularly peat, and correction schemes for partial pixel obstructions due to cloud or haze have strong qualitative and quantitative effects on emissions and resulting pollution levels. Future work will aim toward an improvement of the MSS emission data by making use of FRP observations that are processed by GFAS and therefore include cloud-cover corrections and plume-rise information. Further improvements of the representation of fire activity may be gained from including a diurnal burning cycle. Combining the spatially much better resolved information from polar-orbiting satellites with time-resolved information from geostationary satellite retrievals will also be vital for a truly quantitative forecast of biomass burning in Southeast Asia.

Appendix A: Validation Metrics

The following validation metrics were used for a quantitative evaluation of dispersion simulation accuracies presented in section 4:

1. Factor of 2 of observations:

$$FAC2 = \frac{1}{N} \sum_i \Phi_i \quad \text{with} \quad \Phi_i = \begin{cases} 1, & \text{if } \frac{1}{2} \leq \frac{M_i}{O_i} \leq 2. \\ 0, & \text{otherwise.} \end{cases}$$

2. Modified normalized mean bias:

$$MNMB = \frac{2}{N} \sum_i \left(\frac{M_i - O_i}{M_i + O_i} \right).$$

3. Fractional gross error:

$$FRG = \frac{2}{N} \sum_i \left| \frac{M_i - O_i}{M_i + O_i} \right|.$$

4. Correlation coefficient:

$$R = \frac{\frac{1}{N} \sum_i (M_i - \bar{M})(o_i - \bar{o})}{\sigma_M \sigma_o}$$

Here M denotes the simulation (forecast) results and o the observations. In the case of this study, i denotes a time index at a specific site. FAC2 provides a measure of the fraction of modeled PM_{10} concentrations that are within a factor of 2 of the observed values. In order to evaluate simulation bias and errors, we use metrics that are commonly employed to evaluate forecast accuracies of air quality models [e.g., Ordóñez *et al.*, 2010; Savage *et al.*, 2013]. As discussed by Savage *et al.* [2013], normalized bias and error metrics like the MNMB or FGE provide consistent accuracy scales independent of pollutant type and concentration threshold values. Using the arithmetic mean of observed and modeled concentration values for the normalization, MNMB treats model deficiencies in terms of overprediction and underprediction trends in a symmetric manner [Cox and Tikvart, 1990]. The MNMB is bounded on the interval $[-2, +2]$. The FGE represents a normalized version of the mean absolute error of the simulation. It indicates the overall forecast error and also behaves symmetrically with regard to overpredictions and underpredictions. The FGE is bounded on the interval $[0, +2]$. For both MNMB and FGE, a value of 0 indicates a flawless simulation. The correlation coefficient is consulted in order to determine the extent to which trends and patterns in the simulation are matching those present in the observations.

Acknowledgments

The authors thank Singapore's National Environment Agency, the Pollution Control Department of the Ministry Natural Resources and Environment of Thailand (www.aqmthai.com), and the Department of Environment of Malaysia (<http://apims.doe.gov.my/apims/hourly3.php>) for providing surface measurements of PM_{10} for the analyses in this study. We are thankful for the support from the GFAS developers in using the GFAS v1.2 emission data set (http://www.copernicus-atmosphere.eu/about/project_structure/input_data/d_fire/gfas_versions/). We would like to thank the Centre for Remote Imaging, Sensing and Processing (CRISP) at the National University of Singapore for providing the 250 m resolution 2010 land cover map of Insular Southeast Asia. We would also like to thank colleagues in the Met Office's Air Quality and Composition team for helpful discussions about operational bias correction and forecast verification approaches. Processed data, analysis results, and analysis and visualization codes are available upon request from the Met Office (email to atmospheric.dispersion@metoffice.gov.uk).

References

- Akagi, S. K., R. J. Yokelson, C. Wiedinmyer, M. J. Alvarado, J. S. Reid, T. Karl, J. D. Crouse, and P. O. Wennberg (2011), Emission factors for open and domestic biomass burning for use in atmospheric models, *Atmos. Chem. Phys.*, *11*(9), 4039–4072, doi:10.5194/acp-11-4039-2011.
- Andela, N., J. W. Kaiser, A. Heil, T. van Leeuwen, M. Wooster, G. van der Werf, S. Remy, and M. Schultz (2013), Assessment of the global fire assimilation system (GFASv1), *Tech. Memo. 702*, ECMWF, Reading, U. K.
- Andreae, M. O., and P. Merlet (2001), Emission of trace gases and aerosols from biomass burning, *Global Biogeochem. Cycles*, *15*(4), 955–966, doi:10.1029/2000GB001382.
- Atwood, S. A., J. S. Reid, S. M. Kreidenweis, L. E. Yu, S. V. Salinas, B. N. Chew, and R. Balasubramanian (2013), Analysis of source regions for smoke events in Singapore for the 2009 El Niño burning season, *Atmos. Environ.*, *78*, 219–230, doi:10.1016/j.atmosenv.2013.04.047.
- Balasubramanian, R., T. Victor, and R. Begum (1999), Impact of biomass burning on rainwater acidity and composition in Singapore, *J. Geophys. Res.*, *104*(D21), 26,881–26,890, doi:10.1029/1999JD900247.
- Benedetti, A., et al. (2009), Aerosol analysis and forecast in the European Centre for Medium-Range Weather Forecasts Integrated Forecast System: 2. Data assimilation, *J. Geophys. Res.*, *114*, D13205, doi:10.1029/2008JD011115.
- Borrego, C., A. Monteiro, M. T. Pay, I. Ribeiro, A. I. Miranda, S. Basart, and J. M. Baldasano (2011), How bias-correction can improve air quality forecasts over Portugal, *Atmos. Environ.*, *45*(37), 6629–6641, doi:10.1016/j.atmosenv.2011.09.006.
- Byun, D., and K. L. Schere (2006), Review of the governing equations, computational algorithms, and other components of the Models-3 Community Multiscale Air Quality (CMAQ) modeling system, *Appl. Mech. Rev.*, *59*(2), 51–77, doi:10.1115/1.2128636.
- Chang, C.-P., Z. Wang, J. McBride, and C.-H. Lu (2005), Annual cycle of Southeast Asia–Maritime Continent rainfall and the asymmetric monsoon transition, *J. Clim.*, *18*, 287–301, doi:10.1175/JCLI-3257.1.
- Chew, B. N., J. R. Campbell, S. V. Salinas, C. W. Chang, J. S. Reid, E. J. Welton, B. N. Holben, and S. C. Liew (2013), Aerosol particle vertical distributions and optical properties over Singapore, *Atmos. Environ.*, *79*, 599–613, doi:10.1016/j.atmosenv.2013.06.026.
- Christian, T. J., B. Kleiss, R. J. Yokelson, R. Holzinger, P. J. Crutzen, W. M. Hao, B. H. Saharjo, and D. E. Ward (2003), Comprehensive laboratory measurements of biomass-burning emissions: 1. Emissions from Indonesian, African, and other fuels, *J. Geophys. Res.*, *108*(D23), 4719, doi:10.1029/2003JD003704.
- Cox, W. M., and J. A. Tikvart (1990), A statistical procedure for determining the best performing air quality simulation model, *Atmos. Environ.*, *24*(9), 2387–2395, doi:10.1016/0960-1686(90)90331-G.
- Darmenov, A., and A. da Silva (2013), The Quick Fire Emissions Dataset (QFED)—Documentation of versions 2.1, 2.2 and 2.4, in *NASA Technical Report Series on Global Modeling and Data Assimilation TM-2014-104606*, vol. 32, edited by M. J. Suarez, pp. 1–183, NASA, USA.
- Davies, T., M. J. P. Cullen, A. J. Malcolm, M. H. Mawson, A. Staniforth, A. A. White, and N. Wood (2005), A new dynamical core for the Met Office's global and regional modelling of the atmosphere, *Q. J. R. Meteorol. Soc.*, *131*(608), 1759–1782, doi:10.1256/qj.04.101.
- Draxler, R., et al. (2015), World Meteorological Organization's model simulations of the radionuclide dispersion and deposition from the Fukushima Daiichi nuclear power plant accident, *J. Environ. Radioact.*, *139*, 172–184, doi:10.1016/j.jenvrad.2013.09.014.
- Emmanuel, S. C. (2000), Impact to lung health of haze from forest fires: The Singapore experience, *Respirology*, *5*(2), 175–182, doi:10.1046/j.1440-1843.2000.00247.x.
- Field, R. D., G. R. van der Werf, and S. S. P. Shen (2009), Human amplification of drought-induced biomass burning in Indonesia since 1960, *Nat. Geosci.*, *2*(3), 185–188, doi:10.1038/ngeo443.
- Frankenberger, E., D. McKee, and D. Thomas (2005), Health consequences of forest fires in Indonesia, *Demography*, *42*(1), 109–129.
- Freitas, S. R., K. M. Longo, R. Chatfield, D. Latham, M. A. F. Silva Dias, M. O. Andreae, E. Prins, J. C. Santos, R. Gielow, and J. A. Carvalho Jr. (2007), Including the sub-grid scale plume rise of vegetation fires in low resolution atmospheric transport models, *Atmos. Chem. Phys.*, *7*(13), 3385–3398, doi:10.5194/acp-7-3385-2007.
- Fuller, D. O., and K. Murphy (2006), The ENSO-fire dynamic in insular southeast Asia, *Clim. Change*, *74*(4), 435–455, doi:10.1007/s10584-006-0432-5.
- Gautam, R., N. C. Hsu, T. F. Eck, B. N. Holben, S. Janjai, T. Jantarach, S.-C. Tsay, and W. K. Lau (2013), Characterization of aerosols over the Indochina peninsula from satellite-surface observations during biomass burning pre-monsoon season, *Atmos. Environ.*, *78*, 51–59, doi:10.1016/j.atmosenv.2012.05.038.

- Gaveau, D. L. A., et al. (2014), Major atmospheric emissions from peat fires in Southeast Asia during non-drought years: Evidence from the 2013 Sumatran fires, *Sci. Rep.*, *4*, 6112, doi:10.1038/srep06112.
- Giglio, L., J. Descloitres, C. O. Justice, and Y. J. Kaufman (2003), An enhanced contextual fire detection algorithm for MODIS, *Remote Sens. Environ.*, *87*, 273–282, doi:10.1016/S0034-4257(03)00184-6.
- Giglio, L., I. Csizsar, and C. O. Justice (2006), Global distribution and seasonality of active fires as observed with the Terra and Aqua Moderate Resolution Imaging Spectroradiometer (MODIS) sensors, *J. Geophys. Res.*, *111*, G02016, doi:10.1029/2005JG000142.
- Goldammer, J. G. (1997), The role of fire on greenhouse gas and aerosol emissions and land use and cover change in Southeast Asia: Ecological background and research needs, paper presented at the International Conference on Science and Technology for the Assessment of Global Environmental Change and its Impacts on the Indonesian Maritime Continent, Jakarta, Indonesia, 10–12 Nov.
- Hansen, M. C., et al. (2013), High-resolution global maps of 21st-century forest cover change, *Science*, *342*(6160), 850–853, doi:10.1126/science.1244693.
- Heil, A., and J. Goldammer (2001), Smoke-haze pollution: A review of the 1997 episode in Southeast Asia, *Reg. Environ. Change*, *2*(1), 24–37, doi:10.1007/s101130100021.
- Heil, A., B. Langmann, and E. Aldrian (2007), Indonesian peat and vegetation fire emissions: Study on factors influencing large-scale smoke haze pollution using a regional atmospheric chemistry model, *Mitig. Adapt. Strategies Global Change*, *12*(1), 113–133, doi:10.1007/s11027-006-9045-6.
- Heil, A., J. W. Kaiser, G. R. van der Werf, M. J. Wooster, M. G. Schultz, and H. D. van der Gon (2010), Assessment of the real-time fire emissions (GFASv0) by MACC, *Tech. Memo. 628*, ECMWF, Reading, U. K.
- Hoare, P. (2004), A process for community and government cooperation to reduce the forest fire and smoke problem in Thailand, *Agric. Ecosyst. Environ.*, *104*(1), 35–46, doi:10.1016/j.agee.2004.01.036.
- Huang, K., J. S. Fu, N. C. Hsu, Y. Gao, X. Dong, S.-C. Tsay, and Y. F. Lam (2013), Impact assessment of biomass burning on air quality in Southeast and East Asia during BASE-ASIA, *Atmos. Environ.*, *78*, 291–302, doi:10.1016/j.atmosenv.2012.03.048.
- Hyer, E. J., and B. N. Chew (2010), Aerosol transport model evaluation of an extreme smoke episode in Southeast Asia, *Atmos. Environ.*, *44*(11), 1422–1427, doi:10.1016/j.atmosenv.2010.01.043.
- Hyer, E. J., J. S. Reid, E. M. Prins, J. P. Hoffman, C. C. Schmidt, J. I. Miettinen, and L. Giglio (2013), Patterns of fire activity over Indonesia and Malaysia from polar and geostationary satellite observations, *Atmos. Res.*, *122*, 504–519, doi:10.1016/j.atmosres.2012.06.011.
- Ichoku, C., and L. Ellison (2014), Global top-down smoke-aerosol emissions estimation using satellite fire radiative power measurements, *Atmos. Chem. Phys.*, *14*(13), 6643–6667, doi:10.5194/acp-14-6643-2014.
- Ichoku, C., and Y. J. Kaufman (2005), A method to derive smoke emission rates from MODIS fire radiative energy measurements, *IEEE Trans. Geosci. Remote Sens.*, *43*(11), 2636–2649, doi:10.1109/TGRS.2005.857328.
- Johnson, B. T., S. R. Osborne, J. M. Haywood, and M. A. J. Harrison (2008), Aircraft measurements of biomass burning aerosol over West Africa during DABEX, *J. Geophys. Res.*, *113*, D00C06, doi:10.1029/2007JD009451.
- Jones, A., D. Thomson, M. Hort, and B. Devenish (2007), The U.K. Met Office's next-generation atmospheric dispersion model, NAME III, in *Air Pollution Modeling and Its Application XVII*, edited by C. Borrego and A.-L. Norman, pp. 580–589, Springer, New York.
- Jones, D. S. (2006), ASEAN and transboundary haze pollution in Southeast Asia, *Asia Eur. J.*, *4*(3), 431–446, doi:10.1007/s10308-006-0067-1.
- Kaiser, J. W., et al. (2012), Biomass burning emissions estimated with a global fire assimilation system based on observed fire radiative power, *Biogeosciences*, *9*(1), 527–554, doi:10.5194/bg-9-527-2012.
- Kaiser, J. W., et al. (2014), Recommended fire emission service enhancements, *Tech. Memo. 724*, ECMWF, Reading, U. K.
- Kang, D., R. Mathur, S. T. Rao, and S. Yu (2008), Bias adjustment techniques for improving ozone air quality forecasts, *J. Geophys. Res.*, *113*, D23308, doi:10.1029/2008JD010151.
- Kim, P. S., D. J. Jacob, L. J. Mickley, S. N. Kopplitz, M. E. Marlier, R. S. DeFries, S. S. Myers, B. N. Chew, and Y. H. Mao (2015), Sensitivity of population smoke exposure to fire locations in Equatorial Asia, *Atmos. Environ.*, *102*, 11–17, doi:10.1016/j.atmosenv.2014.09.045.
- Koe, L. C. C., A. F. Arellano Jr., and J. L. McGregor (2001), Investigating the haze transport from 1997 biomass burning in Southeast Asia: Its impact upon Singapore, *Atmos. Environ.*, *35*(15), 2723–2734, doi:10.1016/S1352-2310(00)00395-2.
- Kopplitz, S., L. Mickley, D. Jacob, P. Kim, R. DeFries, M. Marlier, J. Schwartz, J. Buonocore, and S. Myers (2014), Singapore haze in June 2013: Consequences of land use change, fires, and anomalous meteorology for air quality in equatorial Asia. paper presented at the 2014 Fall Meeting, AGU, San Francisco, Calif., 15–19 Dec.
- Kunii, O., S. Kanagawa, I. Yajima, Y. Hisamatsu, S. Yamamura, T. Amagai, and I. T. S. Ismail (2002), The 1997 haze disaster in Indonesia: Its air quality and health effects, *Arch. Environ. Health*, *57*(1), 16–22, doi:10.1080/00039890209602912.
- Lau, K. M., and S. Yang (1997), Climatology and interannual variability of the Southeast Asian summer monsoon, *Adv. Atmos. Sci.*, *14*(2), 141–162, doi:10.1007/s00376-997-0016-y.
- Lin, J., D. Brunner, C. Gerbig, A. Stohl, A. Luhar, and P. Webley (Eds.) (2013), Lagrangian modeling of the atmosphere, *Geophys. Monogr. Ser.*, vol. 200, AGU, Washington, D. C., doi:10.1029/GM200.
- Lohman, D. J., D. Bickford, and N. S. Sodhi (2007), The burning issue, *Science*, *316*(5823), 376, doi:10.1126/science.1140278.
- Marlier, M. E., R. S. DeFries, A. Voulgarakis, P. L. Kinney, J. T. Randerson, D. T. Shindell, Y. Chen, and G. Faluvegi (2013), El Niño and health risks from landscape fire emissions in Southeast Asia, *Nat. Clim. Change*, *3*, 131–136, doi:10.1038/nclimate1658.
- Miettinen, J., C. Shie, and S. C. Liew (2011), Deforestation rates in insular Southeast Asia between 2000 and 2010, *Global Change Biol.*, *17*(7), 2261–2270, doi:10.1111/j.1365-2486.2011.02398.x.
- Miettinen, J., C. Shi, W. J. Tan, and S. C. Liew (2012), 2010 land cover map of insular Southeast Asia in 250m spatial resolution, *Remote Sens. Lett.*, *3*, 11–20, doi:10.1080/01431161.2010.526971.
- Milton, S., J. Heming, R. North, and M. Willett (2015), Performance of the Met Office global NWP prediction system over South East Asia and Tropics, *Internal Rep. (v1.0)*, Met Office, Exeter, U. K.
- Morcrette, J.-J., et al. (2009), Aerosol analysis and forecast in the European Centre for Medium-Range Weather Forecasts Integrated Forecast System: Forward modeling, *J. Geophys. Res.*, *114*, D06206, doi:10.1029/2008JD011235.
- Nachtergaele, F., H. van Velthuis, L. Verelst, and D. Wiberg (2012), Harmonized world soil database (version 1.2). Documentation, FAO/IIASA/ISRIC/ISSCAS/JRC, FAO, Rome, Italy and IIASA, Laxenburg, Austria.
- National Environment Agency (2013), Singapore affected by severe transboundary smoke haze in June 2013. World Meteorological Organization (WMO), News from Members 20 Sept. 2013, Technical document from Singapore's National Environment Agency (NEA). [Available at https://www.wmo.int/pages/mediacentre/news_members/documents/SingaporeAffectedbySevereTransboundarySmokeHazeinJune2013.pdf].
- Neal, L. S., P. Agnew, S. Moseley, C. Ordóñez, N. Savage, and M. Tilbee (2014), Application of a statistical post-processing technique to a gridded, operational, air quality forecast, *Atmos. Environ.*, *98*, 385–393, doi:10.1016/j.atmosenv.2014.09.004.

- Nichol, J. (1997), Bioclimatic impacts of the 1994 smoke haze event in Southeast Asia, *Atmos. Environ.*, *31*(8), 1209–1219, doi:10.1016/S1352-2310(96)00260-9.
- Nodzu, M. I., S.-Y. Ogino, Y. Tachibana, and M. D. Yamanaka (2006), Climatological description of seasonal variations in lower-tropospheric temperature inversion layers over the Indochina Peninsula, *J. Clim.*, *19*(13), 3307–3319, doi:10.1175/JCLI3792.1.
- Nodzu, M. I., S.-Y. Ogino, and M. D. Yamanaka (2011), Seasonal changes in a vertical thermal structure producing stable lower-troposphere layers over the Inland Region of the Indochina Peninsula, *J. Clim.*, *24*(13), 3211–3223, doi:10.1175/2010JCLI3871.1.
- Ordóñez, C., et al. (2010), Global model simulations of air pollution during the 2003 European heat wave, *Atmos. Chem. Phys.*, *10*(2), 789–815, doi:10.5194/acp-10-789-2010.
- Page, S. E., F. Siegert, J. Rieley, H.-D. V. Boehm, A. Jaya, and S. Limin (2002), The amount of carbon released from peat and forest fires in Indonesia during 1997, *Nature*, *420*, 61–65, doi:10.1038/nature01131.
- Ramage, C. (1968), Role of a tropical “maritime continent” in the atmospheric circulation, *Mon. Weather Rev.*, *96*, 365–370.
- Reddington, C. L., M. Yoshioka, R. Balasubramanian, D. Ridley, Y. Y. Toh, S. R. Arnold, and D. V. Spracklen (2014), Contribution of vegetation and peat fires to particulate air pollution in Southeast Asia, *Environ. Res. Lett.*, *9*(9), 094006, doi:10.1088/1748-9326/9/9/094006.
- Reid, J. S., R. Koppmann, T. F. Eck, and D. P. Eleuterio (2005), A review of biomass burning emissions. Part II: Intensive physical properties of biomass burning particles, *Atmos. Chem. Phys.*, *5*(3), 799–825, doi:10.5194/acp-5-799-2005.
- Reid, J. S., et al. (2009), Global monitoring and forecasting of biomass-burning smoke: Description of and lessons from the Fire Locating and Modeling of Burning Emissions (FLAMBE) program, *IEEE J. Sel. Top. Appl.*, *2*(3), 144–162, doi:10.1109/JSTARS.2009.2027443.
- Reid, J. S., P. Xian, E. J. Hyer, M. K. Flatau, E. M. Ramirez, F. J. Turk, C. R. Sampson, C. Zhang, E. M. Fukada, and E. D. Maloney (2012), Multi-scale meteorological conceptual analysis of observed active fire hotspot activity and smoke optical depth in the Maritime Continent, *Atmos. Chem. Phys.*, *12*(4), 2117–2147, doi:10.5194/acp-12-2117-2012.
- Reid, J. S., et al. (2013), Observing and understanding the Southeast Asian aerosol system by remote sensing: An initial review and analysis for the Seven Southeast Asian Studies (7SEAS) program, *Atmos. Res.*, *122*, 403–468, doi:10.1016/j.atmosres.2012.06.005.
- Rienecker, M. M., et al. (2008), The GEOS-5 data assimilation system—Documentation of versions 5.0.1, 5.1.0, and 5.2.0, *Tech. Memo. 2007-104606*, vol. 27, NASA, Greenbelt, Md.
- Rolph, G. D., et al. (2009), Description and verification of the NOAA smoke forecasting system: The 2007 fire season, *Weather Forecasting*, *24*, 361–378, doi:10.1175/2008WAF2222165.1.
- Savage, N. H., P. Agnew, L. S. Davis, C. Ordóñez, R. Thorpe, C. E. Johnson, F. M. O’Connor, and M. Dalvi (2013), Air quality modelling using the Met Office Unified Model (AQUUM OS24-26): Model description and initial evaluation, *Geosci. Model Dev.*, *6*(2), 353–372, doi:10.5194/gmd-6-353-2013.
- Selvaradjou, S.-K., L. Montanarella, O. Spaargaren, D. Dent, N. Filippi, and S. Dominik (2005), European Digital Archive of Soil Maps (EuDASM)—Metadata of the soil maps of Asia, *EUR 21820 EN*, Off. for Off. Publ. of the European Communities, Luxembourg.
- Sessions, W. R., et al. (2015), Development towards a global operational aerosol consensus: Basic climatological characteristics of the International Cooperative for Aerosol Prediction Multi-Model Ensemble (ICAP-MME), *Atmos. Chem. Phys.*, *15*, 335–362, doi:10.5194/acp-15-335-2015.
- Simmonds, P. G., A. J. Manning, R. G. Derwent, P. Ciais, M. Ramonet, V. Kazan, and D. Ryall (2005), A burning question. Can recent growth rate anomalies in the greenhouse gases be attributed to large-scale biomass burning events?, *Atmos. Environ.*, *39*(14), 2513–2517, doi:10.1016/j.atmosenv.2005.02.018.
- Sirimongkonlertkul, N., and V. Phonekeo (2012), Remote sensing and GIS application analysis of active fire, aerosol optical thickness and estimated PM10 in the North of Thailand and Chiang Rai Province, *APCBEE Procedia*, *1*, 304–308, doi:10.1016/j.apcbee.2012.03.050.
- Stott, P. (1986), The spatial pattern of dry season fires in the savanna forests of Thailand, *J. Biol.*, *13*(4), 345–358.
- Strand, T. M., N. Larkin, K. J. Craig, S. Raffuse, D. Sullivan, R. Solomon, M. Rorig, N. Wheeler, and D. Pryden (2012), Analyses of BlueSky Gateway PM2.5 predictions during the 2007 southern and 2008 northern California fires, *J. Geophys. Res.*, *117*, D17301, doi:10.1029/2012JD017627.
- Streets, D. G., K. F. Yarber, J.-H. Woo, and G. R. Carmichael (2003), Biomass burning in Asia: Annual and seasonal estimates and atmospheric emissions, *Global Biogeochem. Cycles*, *17*(4), 1099, doi:10.1029/2003GB002040.
- Tanaka, T. Y., K. Orito, T. T. Sekiyama, K. Shibata, M. Chiba, and H. Tanaka (2003), MASINGAR: A global tropospheric aerosol chemical transport model coupled with MRI/JMA98 GCM: Model description, *Pap. Meteorol. Geophys.*, *53*, 119–138.
- Taylor, D. (2010), Biomass burning, humans and climate change in Southeast Asia, *Biodivers. Conserv.*, *19*(4), 1025–1042, doi:10.1007/s10531-009-9756-6.
- Tosca, M. G., J. T. Randerson, C. S. Zender, D. L. Nelson, D. J. Diner, and J. A. Logan (2011), Dynamics of fire plumes and smoke clouds associated with peat and deforestation fires in Indonesia, *J. Geophys. Res.*, *116*, D08207, doi:10.1029/2010JD015148.
- van der Werf, G. R., J. T. Randerson, G. J. Collatz, L. Giglio, P. S. Kasibhatla, A. F. Arellano Jr., S. C. Olsen, and E. S. Kasichke (2004), Continental-scale partitioning of fire emissions during the 1997 to 2001 El Niño/La Niña period, *Science*, *303*(5654), 73–76, doi:10.1126/science.1090753.
- van der Werf, G. R., J. T. Randerson, L. Giglio, G. J. Collatz, M. Mu, P. S. Kasibhatla, D. C. Morton, R. S. DeFries, Y. Jin, and T. T. van Leeuwen (2010), Global fire emissions and the contribution of deforestation, savanna, forest, agricultural, and peat fires (1997–2009), *Atmos. Chem. Phys.*, *10*(23), 11,707–11,735, doi:10.5194/acp-10-11707-2010.
- Wahyunto, S. R., and H. Subagio (2003), *Maps of Area of Peatland Distribution and Carbon Content in Sumatra, 1990–2002*, Wetlands International – Indonesia Programme and Wildlife Habitat Canada (WHC), Bogor, Indonesia.
- Wahyunto, S. R., and H. Subagio (2004), *Maps of Area of Peatland Distribution and Carbon Content in Kalimantan, 2000–2002*, Wetlands International – Indonesia Programme and Wildlife Habitat Canada (WHC), Bogor, Indonesia.
- Wang, J., C. Ge, Z. Yang, E. J. Hyer, J. S. Reid, B.-N. Chew, M. Mahmud, Y. Zhang, and M. Zhang (2013), Mesoscale modeling of smoke transport over the Southeast Asian Maritime Continent: Interplay of sea breeze, trade wind, typhoon, and topography, *Atmos. Res.*, *122*, 486–503, doi:10.1016/j.atmosres.2012.05.009.
- Webster, H. N., et al. (2012), Operational prediction of ash concentrations in the distal volcanic cloud from the 2010 Eyjafjallajökull eruption, *J. Geophys. Res.*, *117*, D00U08, doi:10.1029/2011JD016790.
- Wiedinmyer, C., S. K. Akagi, R. J. Yokelson, L. K. Emmons, J. A. Al-Saadi, J. J. Orlando, and A. J. Soja (2011), The Fire INventory from NCAR (FINN): A high resolution global model to estimate the emissions from open burning, *Geosci. Model Dev.*, *4*(3), 625–641, doi:10.5194/gmd-4-625-2011.
- Witham, C., and A. Manning (2007), Impacts of Russian biomass burning on UK air quality, *Atmos. Environ.*, *41*(37), 8075–8090, doi:10.1016/j.atmosenv.2007.06.058.

- Wooster, M., B. Zhukov, and D. Oertel (2003), Fire radiative energy for quantitative study of biomass burning: Derivation from the BIRD experimental satellite and comparison to MODIS fire products, *Remote Sens. Environ.*, *86*(1), 83–107, doi:10.1016/S0034-4257(03)00070-1.
- Wooster, M. J., G. Roberts, G. L. W. Perry, and Y. J. Kaufman (2005), Retrieval of biomass combustion rates and totals from fire radiative power observations: FRP derivation and calibration relationships between biomass consumption and fire radiative energy release, *J. Geophys. Res.*, *110*, D24311, doi:10.1029/2005JD006318.
- Xian, P., J. S. Reid, J. Turk, E. J. Hyer, and D. L. Westphal (2009), Impact of modeled versus satellite measured tropical precipitation on regional smoke optical thickness in an aerosol transport model, *Geophys. Res. Lett.*, *36*, L16805, doi:10.1029/2009GL038823.
- Xian, P., J. S. Reid, S. A. Atwood, R. S. Johnson, E. J. Hyer, D. L. Westphal, and W. Sessions (2013), Smoke aerosol transport patterns over the Maritime Continent, *Atmos. Res.*, *122*, 469–485, doi:10.1016/j.atmosres.2012.05.006.
- Yulianti, N., and H. Hayasaka (2013), Recent active fires under El Niño conditions in Kalimantan, Indonesia, *Am. J. Plant Sci.*, *4*(3A), 685–696, doi:10.4236/ajps.2013.43A087.
- Yulianti, N., H. Hayasaka, and A. Sepriando (2013), Recent trends of fire occurrence in Sumatra (analysis using MODIS hotspot data): A comparison with fire occurrence in Kalimantan, *Open J. For.*, *3*, 129–137, doi:10.4236/ojf.2013.34021.
- Zhang, F., et al. (2014), Sensitivity of mesoscale modeling of smoke direct radiative effect to the emission inventory: A case study in northern sub-Saharan African region, *Environ. Res. Lett.*, *9*, 075002, doi:10.1088/1748-9326/9/7/075002.
- Zhang, J., J. S. Reid, D. L. Westphal, N. L. Baker, and E. J. Hyer (2008), A system for operational aerosol optical depth data assimilation over global oceans, *J. Geophys. Res.*, *113*, D10208, doi:10.1029/2007JD009065.
- Zhang, Y., T. Li, B. Wang, and G. Wu (2002), Onset of the summer monsoon over the Indochina Peninsula: Climatology and interannual variations, *J. Clim.*, *15*(22), 3206–3221.